JM PAPERS

Aerothermodynamics of a sphere in a monatomic gas based on *ab initio* interatomic potentials over a wide range of gas rarefaction: transonic, supersonic and hypersonic flows

Felix Sharipov[1],[†] **and Alexey N. Volkov**[2]

[1]Departamento de Física, Universidade Federal do Paraná, Caixa Postal 19044, Curitiba 81531-980, Brazil

[2]Department of Mechanical Engineering, University of Alabama, H.M. Comer Hall, 7th Avenue, Tuscaloosa, AL 35487, USA

Aerothermodynamic characteristics of a sphere such as drag and energy transfer coefficients are calculated for Mach numbers varying from 1 to 10 over a wide range of the gas rarefaction degree spanning the free molecular, transitional and near hydrodynamic flow regimes. The effects of major factors determining the gas flow are studied using the direct simulation Monte Carlo method. To reveal the effect of gas species, the simulations are performed based on *ab initio* interatomic potentials for helium, neon, argon and krypton, as well as based on the hard sphere model. The impact of the accommodation coefficients is evaluated by applying the Cercignani–Lampis model of gas–surface interaction. The calculations are carried out for several values of the free stream and sphere temperatures. It is found that the effects of gas species on the drag and energy transfer coefficients are approximately 3 % and 6 %, respectively. The accommodation coefficients in the Cercignani–Lampis model strongly affect all aerothermodynamic characteristics. The drag and energy transfer coefficients calculated for different accommodation coefficients vary within 30 % and 200 %, respectively. It is found that the variation of the tangential momentum and normal energy accommodation coefficients can induce an increase of the drag coefficient compared to the case of diffuse gas–surface interaction. In hypersonic flows, the drag coefficient varies within 30 % when the sphere temperature varies from the free stream temperature to the stagnation temperature. The drag and energy transfer coefficients are found to be non-monotonic functions of the free stream temperature.

Key words: high-speed flow, supersonic flow

---

† Email address for correspondence: sharipov@fisica.ufpr.br

1. Introduction

A gas flow past a sphere is a fundamental problem of fluid dynamics. The solution to this problem for subsonic flows at low Reynolds numbers in the Stokes regime is well known and can be found in numerous textbooks (see e.g. Landau & Lifshitz 1989; Batchelor 2000). Supersonic and hypersonic flows past a sphere in the continuum flow regime were the subject of numerous experimental and computational studies (see e.g. Nagata *et al.* 2016, 2018, 2020; Loth *et al.* 2021, and references therein). In this case, a supersonic flow always implies a high Reynolds number. Transonic and supersonic flows at low Reynolds numbers occur when a sphere moves with a velocity near or above the speed of sound through a low-density rarefied gas, where the mean free path of gas molecules is comparable to or larger than the sphere radius. Such flow conditions are typical at re-entry of space vehicles (Dogra, Wilmoth & Moss 1992; Storch 2002), impact ejecta and meteoroids (Melosh & Goldin 2008), for small solid particles in two-phase flows in solid-propellant engines, jets and plumes (Carlson & Hoglund 1964; Crowe 1967; Nelson & Fields 1996; Crowe, Sommerfeld & Tsuji 1998), and in the shock layers in front of bodies moving with supersonic speed in the dusty Earth (Vasilevskii *et al.* 2001) and Martian (Papadopoulos, Tauber & Chang 1993; Ozawa *et al.* 2011; Ching, Barnhardt & Ihme 2021) atmospheres. These examples predetermine the practical interest to supersonic and hypersonic low-Reynolds-number flows over spheres, since the model of a spherical body is considered as the most general and common geometrical model for spacecrafts, meteoroids and dust particles. Due to the fundamental nature of this problem, the flow past a sphere can be considered as one of the benchmark problems of rarefied gas dynamics (Sharipov 2012) and can be used to validate various numerical methods.

Continuum supersonic and hypersonic flows over a sphere are characterized by the formation of a bow shock wave in front of the body, a boundary layer at its surface, and flow separation that induces unsteady wakes behind the sphere. These flow features affect directly the two most important aerothermodynamic properties of a sphere, its drag force and energy transfer rate. When the gas density in the free stream or the size of a sphere gradually decreases, the effects of gas rarefaction become important. Due to gas rarefaction, the thicknesses of both bow shock wave and boundary layer increase, so that they merge smoothly into a viscous layer (Vogenitz *et al.* 1968), and the degree of unsteadiness of the wake flow reduces (Dogra *et al.* 1994). For continuum flows past a sphere, an increase in the Mach number also reduces the degree of the wake unsteadiness (Nagata *et al.* 2016). In particular, three-dimensional simulations by Riahia *et al.* (2018) based on the compressible Navier–Stokes equations showed that the flow past a sphere is axisymmetric and steady at Mach number 2 and Reynolds number lower than 600. The continuum simulations and bifurcation analysis also show that the supersonic flow past a sphere remains globally stable at least for Reynolds numbers below 370 (Sansica *et al.* 2018).

In a rarefied gas, the frequency of intermolecular collisions drops, so that the assumption of local equilibrium no longer holds. Then the continuum hypothesis breaks down (Lofthouse, Boyd & Wright 2007) and the flow cannot be described by the Navier–Stokes equations. Under such conditions, the flow regime is referred to as transitional, and the flow past a sphere can be described by mathematical models based on the Boltzmann kinetic equation (Hirschfelder, Curtiss & Bird 1954; Ferziger & Kaper 1972; Cercignani 1975; Sharipov 2016). One of the computational methods to solve problems based on the Boltzmann equation is the direct simulation Monte Carlo (DSMC) method (Bird 1994, 2013). The DSMC method is a stochastic particle-based method, where the flow of a dilute gas is described by multiple simulated or modelling particles, which move and interact

with each other like individual gas molecules in a real gas flow. The most important part of the DSMC method, the scheme for sampling binary collisions between simulated particles, is derived in agreement with the collision term in the Boltzmann equation. Therefore, the DSMC method is capable of providing unbiased statistical estimates for the solutions of the Boltzmann equation (Wagner 1992).

The DSMC method was used initially by Vogenitz *et al.* (1968) to study two-dimensional supersonic and hypersonic flows past a sphere. They considered, however, only two simulation cases, and some parameters of the computational model were not provided. A hypersonic flow of an oxygen–nitrogen mixture past a sphere was simulated by the DSMC method by Dogra *et al.* (1994). A three-dimensional flow past a rotating sphere is considered by Volkov (2009, 2011) based on the hard sphere model. The recent paper by Loth *et al.* (2021) reports some results on the sphere drag based on the DSMC method without specifying the molecular model parameters. The heat transfer of a sphere was not considered in these works, with exception of papers by Volkov (2009, 2011). Point-to-point comparison of the results obtained in these works is impossible, since the simulations were performed based on different molecular models and at different values of the Mach and Reynolds numbers. Thus the computational data on the sphere drag and heat transfer in the transitional flow regime available from literature are essentially incomplete. Moreover, none of the known DSMC-based studies addressed specifically the effects of gas species, gas–surface interaction parameters, free stream temperature and body temperature in supersonic and hypersonic transitional flows past a sphere.

In the limit of free molecular flow when the gas is highly rarefied and the intermolecular collisions can be neglected, the flow past a sphere can be obtained from a collisionless kinetic equation. The free molecular drag and energy transfer coefficients are functions of the free stream characteristics and parameters of the gas–surface interaction. For the diffuse–specular interaction (Schaaf & Chambre 1961; Kogan 1969; Cercignani 1975; Sharipov 2016), the expressions of the drag and energy transfer coefficients for a sphere are well known (Ashley 1949; Sauer 1951; Bird 1994; Storch 2002). However, this model contains only one parameter, which cannot describe all variety of experimental data. The model proposed by Cercignani & Lampis (1971) contains two accommodation coefficients that allow one to describe the interaction of gas molecules with various treated and non-treated surfaces in quantitative agreement with the results of experimental measurements, and thus to account for the effect of surface state on the aerothermodynamic characteristics of bodies in rarefied gas flow. An approximate expression of the sphere drag coefficient in the free molecular flow regime based on the Cercignani–Lampis (CL) model (Cercignani & Lampis 1971) was suggested by Walker, Mehta & Koller (2014) and Chernyak & Sograbi (2020). The CL model was applied to the gas flow past sphere in the transitional flow regime only at small Mach numbers (Kalempa & Sharipov 2020, 2021). These results indicate the strong dependence of the drag and energy transfer coefficients on parameters of the CL model and surface temperature. Such a strong dependence is also expected to persist in supersonic flows in the transitional flow regime.

The sphere drag coefficient in supersonic flows was measured for the free stream Mach number up to 11 by Wegener & Ashkenas (1961), Kingslow & Potter (1963), Bailey & Hiatt (1971, 1972) and Bailey (1974). The known experimental data, however, correspond to the range of the free stream Reynolds number equal to or greater than 10. These experimental data, together with the approximate theoretical equations for free molecular flow, were used to design multiple semi-empirical correlations for the sphere drag coefficient in a

broad range of Mach and Reynolds numbers. Among others, the correlations proposed by Henderson (1976), Loth (2008) and Loth *et al.* (2021) are used widely to predict drag force exerted on dust particles in supersonic two-phase gas–solid particle flows (see e.g. Volkov, Tsirkunov & Oesterlé 2005; Ching *et al.* 2021). Although multiple corrections were further proposed for these equations to improve the agreement with the experimental data (e.g. Walsh 1977; Parmar, Haselbacher & Balachandar 2010; Loth *et al.* 2021), all known semi-empirical correlations for the sphere drag coefficient suffer from two drawbacks. First, they are not validated against experimental data in the transitional flow regime. Second, they do not account for the effects of gas species and parameters describing incomplete accommodation of gas molecules at the interaction with the sphere surface. The theoretical computations of high-speed flows past a sphere in the transitional flow regime can fill these gaps and provide data for the flow conditions least studied experimentally.

The effects of rarefaction and compressibility on the energy transfer of spheres in supersonic low-Reynolds-number flow were studied experimentally, among others, by Drake & Backer (1952), Kavanau (1955), Avleeva (1970) and Koshmarov & Svirshevskii (1972). Based on the experimental results and known sphere energy transfer in free molecular flow, Sauer (1951), Kavanau (1955) and Koshmarov & Svirshevskii (1972) developed semi-empirical correlations for the sphere energy transfer coefficient applicable in broad ranges of Mach and Reynolds numbers. These equations are often used to predict energy transfer of solid particles in gas–solid particle flows (Carlson & Hoglund 1964; Volkov *et al.* 2005; Ozawa *et al.* 2011; Ching *et al.* 2021). The known experimental data on the sphere energy transfer are even scarcer and less complete than for the sphere drag.

The flows past a sphere, as well as the sphere drag and energy transfer coefficients, in the limit of small Mach number can be calculated theoretically using the variational principles (Cercignani, Pagani & Bassanini 1968), direct numerical solution of the Bhatnagar–Gross–Krook and linearized Boltzmann equations (Lea & Loyalka 1982; Loyalka 1992; Takata, Sone & Aoki 1993), as well as asymptotic expansions of solutions of the Boltzmann equation (Taguchi 2015). Asymptotic methods, however, are not applicable to supersonic flows, so the most reliable tool for simulations of high-speed flows past a sphere in the transitional flow regime is the DSMC method (Bird 1994, 2013).

The flexibility in the implementation of various models of intermolecular and gas–surface interactions is one of the fundamental advantages of the DSMC method. In the present work, the CL scattering kernel is implemented in the DSMC method in the form suggested by Lord (1991). As shown by Sharipov & Strapasson (2012*a*), the DSMC calculations can be performed based on arbitrary interaction potentials for monatomic gases. The use of lookup tables that determine the deflection angle for binary collisions based on the solution of classical (Sharipov & Strapasson 2012*a*, 2013) or quantum mechanical (Sharipov 2018*b*; Dias & Sharipov 2021) scattering problems allows one to perform DSMC calculations with the same computational cost as in the case of the variable hard sphere (VHS) and variable soft sphere (VSS) molecular models (Bird 1994, 2013). The approach based on lookup tables enables modelling interatomic collisions in the DSMC method based on arbitrary interatomic potentials, including the potentials established by *ab initio* (AI) calculations. The works by Sharipov (2018*a*,*b*) showed that at low temperatures, the quantum effects are significant and the lookup tables based on the classical approach lead to wrong results. According to Sharipov (2018*b*), DSMC calculations at any temperature based on the quantum approach require shorter computational time than those based on the classical approach. Therefore, all lookup tables

used in the present work are based on quantum mechanics even when the quantum effects are not significant.

As is known, semi-empirical potentials, such as the hard spheres (HS) model and Lennard-Jones potential, are approximations that contain one or more adjustable parameters. To obtain these parameters, some experimental data, e.g. on the second virial coefficient and viscosity, are used. As a result, the parameter values vary depending on the experimental data utilized for parametrization, therefore the semi-empirical potentials have uncertainties that are hardly estimated. In contrast, the AI potentials are calculated from first physical principles, hence they are free from any adjustable parameter. In this regard, the AI potentials provide a more accurate solution to the scattering problem compared to the semi-empirical potentials such as the Lennard-Jones one. The DSMC method based on AI potentials was used successfully to study energy transfer in a rarefied gas (Strapasson & Sharipov 2014), rarefied gas flow past a circular cylinder (Volkov & Sharipov 2017), the structure of shock waves (Sharipov & Dias 2019; Dias & Sharipov 2021), expansion of laser-induced plumes (Petrov *et al.* 2020), and gaseous mixture flow through an orifice (Sharipov 2017). A systematic comparison of rarefied gas flows based on an AI potential with those based on VHS and VSS models performed by Wang *et al.* (2022) pointed out a significant error of the VHS and VSS models.

The goal of the present work is to perform high-fidelity kinetic simulations of gas flows over a sphere and to reveal the effects of the gas species, parameters of the gas–surface interaction models, free stream temperature and surface temperature on the sphere drag and energy transfer in transonic, supersonic and hypersonic flows of monatomic gases in the transitional flow regime. To this end, we perform systematic simulations of flows based on AI potentials for various noble gases at various degrees of flow rarefaction and free stream/surface temperature ratio in the range of Mach numbers from 1 to 10. The simulations are performed based on AI interatomic interaction potentials obtained by Przybytek *et al.* (2010), Hellmann, Bich & Vogel (2008), Patkowski & Szalewicz (2010) and Jäger *et al.* (2016), as well as the widely used HS molecular model. To study the effects of parameters of gas–surface interaction, we compare the results obtained for diffuse reflection with those based on the CL scattering kernel using the values of the tangential momentum accommodation coefficient (TMAC) and normal energy accommodation coefficient (NEAC) extracted from the experimental data available in the literature (Porodnov *et al.* 1974; Porodnov, Kulev & Tukhvetov 1978; Semyonov, Borisov & Suetin 1984; Trott *et al.* 2011). The calculations were done for various values of the free stream and sphere temperatures. All results are obtained in steady-state two-dimensional axisymmetric simulations, as the three-dimensional and unsteady effects due to the wake instability are known to be negligible under conditions considered here (Nagata *et al.* 2016; Riahia *et al.* 2018; Sansica *et al.* 2018).

A special preliminary study was performed to choose the values of all numerical parameters of the DSMC method, in order to get small and controllable numerical errors of our simulations. This preliminary study is described in the supplementary material available at https://doi.org/10.1017/jfm.2022.356. It allows us to conclude, in particular, that the errors in calculations of the sphere drag and energy transfer coefficients are less than 0.5 % in the whole ranges of Mach and Reynolds numbers considered in our simulations.

Our major finding is that the differences in the drag and energy transfer coefficients between different species calculated based on AI interatomic potentials become progressively more significant with increasing Mach number. The difference reaches its
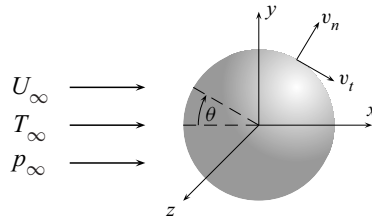
Figure 1. Scheme of the flow.

maximum in the transitional flow regime, while it decreases in the limit of continuum flows. Our simulations also reveal a strong and non-obvious effect of the TMAC and NEAC on the sphere drag and energy transfer. These results suggest that the high-fidelity semi-empirical correlations for the sphere drag and energy transfer coefficients in the transitional flow regime must account for the effect of gas species and parameters of gas–surface interaction.

The rest of the paper is structured as follows. The problem formulation and definitions are presented in § 2. The gas–surface kernel and typical values of the accommodation coefficients are considered in § 3. The drag and heat transfer coefficients of a sphere in free molecular flow based on the CL scattering kernel are obtained and analysed in § 4. The main ideas of implementation of the AI potential into the DSMC method are explained in § 5. Finally, the simulation results are analysed in § 6 and summarized in § 7.

2. Statement of the problem

Consider a sphere of radius R and temperature T_w being at rest and immersed in a dilute monatomic gas. Far from the sphere, in the free stream, the gas at a pressure p_∞ and temperature T_∞ flows with constant velocity U_∞ directed along the x-axis, as shown in figure 1. It is assumed that the stream speed U_∞ is equal to or larger than the speed of sound. The velocity distribution function of the gas in the free stream is given by the Maxwellian

$$f^M_\infty(\boldsymbol{v}) = \frac{n_\infty}{(\sqrt{\pi}v_\infty)^3} \exp\left[-\frac{(v_x - U_\infty)^2 + v_y^2 + v_z^2}{v_\infty^2}\right], \quad v_\infty = \sqrt{\frac{2k_BT_\infty}{m}}, \quad (2.1)$$

where $\boldsymbol{v} = (v_x, v_y, v_z)$ is the molecular velocity, $n_\infty = p_\infty/(k_BT_\infty)$ is the number density, v_∞ is the most probable speed at T_∞, $k_B = 1.380649 \times 10^{-23}\,\mathrm{J\,K^{-1}}$ is the Boltzmann constant, and m is the atomic mass of the gas.

Our purpose is to calculate: the integral characteristics such as the drag force acting on the sphere and energy flux on the sphere surface; the local characteristics on the sphere surface such as the pressure, friction and energy flux coefficients; and, finally, the flow field around the sphere. A wide range of the degree of gas rarefaction spanning the free molecular, transitional and near continuum flow regimes is considered. We study the effect of four factors: the interatomic gas potential of various gas species, accommodation coefficients of the gas–surface interaction model, free stream temperature T_∞, and temperature of the sphere surface T_w. Four gas species will be considered, namely, helium, neon, argon and krypton. Each species has its own interatomic potential so that the comparison of results for different gases reveals the effect of the species on aerothermodynamic characteristics. As pointed out previously by Sharipov (2018*b*), two isotopes of helium, ^{3}He and ^{4}He, have different behaviours at low temperatures. They have

the same interatomic potential, but their collision cross-sections are different. The effect of the helium isotope, therefore, is also studied in the present work by comparison of the results for ^{3}He to those for ^{4}He.

The main factors determining the solution to the problem in question are the Mach number Ma, the rarefaction parameter δ, the ratio of the sphere temperature T_w to the free stream temperature T_∞, and accommodation coefficients. The Mach number is defined as

$$Ma = \frac{U_\infty}{c_s}, \quad c_s = \sqrt{\gamma k_B T_\infty / m}, \tag{2.2}$$

where c_s is the speed of sound, and $\gamma = c_p/c_v$ is the specific energy ratio, which is $\gamma = 5/3$ for monatomic gases. The rarefaction parameter inversely proportional to the Knudsen number is introduced as (Sharipov 2016)

$$\delta = \frac{R p_\infty}{\mu_\infty v_\infty}, \tag{2.3}$$

where μ_∞ is the gas viscosity at the free stream temperature T_∞. The Reynolds number usually defined in continuum fluid mechanics via the sphere diameter ($2R$) is related to Ma and δ as

$$Re = \frac{2R U_\infty \rho_\infty}{\mu_\infty} = 2\sqrt{\frac{10}{3}} \delta Ma, \tag{2.4}$$

where $\rho_\infty = m n_\infty$ is the gas mass density.

In general, the accommodation coefficient α that determines the variation of some quantity $\psi(v)$ associated with a single molecule at gas–surface interaction is defined as (Cercignani 1975; Sharipov 2016)

$$\alpha(\psi) = J_n(\psi)/J_n^{(dif)}(\psi), \tag{2.5}$$

where J_n is the normal flux of the quantity ψ through a solid surface given by

$$J_n(\psi) = \int v_n \psi(v) f(r, v) \, dv; \tag{2.6}$$

$f = f(r, v)$ is the velocity distribution function depending on the position r and molecular velocity v, and v_n is the normal component of v shown in figure 1. The notation $J_n^{(dif)}$ means the flux J_n at the diffuse gas–surface interaction so that $\alpha(\psi) = 1$ for any ψ when the interaction is diffuse. The quantities ψ corresponding to $J_n^{(dif)}(\psi) = 0$, such as $\psi = 1$, should not be used in the definition (2.5). The model of gas–surface interaction used here contains two parameters: TMAC α_t defined via the tangential momentum of gaseous particles $\psi = mv_t$, and NEAC α_n defined via the kinetic energy determined by the velocity component normal to the surface $\psi = mv_n^2/2$. The accommodation coefficients α_t and α_n depend on both gas species and state of the solid surface.

The calculations are performed for Mach numbers $Ma = 1, 2, 5, 10$. The first value belongs to the transonic range of Ma, the second value corresponds to supersonic flow, the third value separates the supersonic and hypersonic flows, and the last value corresponds to hypersonic flow. Five values of the rarefaction parameter, $\delta = 0.1, 0.3, 1, 3, 10, 30$, are considered, spanning the near free molecular, transitional and slip flow regimes. Most of the data are obtained at the free stream temperature $T_\infty = 300$ K. To study the effect of free stream temperature, additional calculations are performed for several T_∞ in the range

Gas	μ (μPa s)	m (u)	G (m s^{-1})
^{3}He	17.2872	3.0160	400
^{4}He	19.9092	4.0026	400
Ne	31.8599	20.180	200
Ar	22.6914	39.948	150
Kr	25.4260	83.798	100

Table 1. Viscosity μ at temperature 300 K (Cencek *et al.* 2012; Sharipov & Benites 2017, 2019, 2020), atomic mass m, and factor G in (5.1) for all gases considered in the present work.

from 1 K to 2000 K. The temperature of the sphere T_w depends on many factors, including thermal properties of the sphere material and its size, and can vary in a broad range. For the flow in question, there are two characteristic temperatures: the free stream temperature T_∞, and the stagnation temperature T_s related to T_∞ as

$$T_s = T_\infty \left(1 + \frac{Ma^2}{3} \right) \tag{2.7}$$

for monatomic gases. Occasionally, a sphere can have T_∞ even at high Ma, for instance, when a supersonic flow arises abruptly in a shock tube. If a sphere is exposed to a hypersonic flow for a long time, then its temperature becomes close to T_s. To account for variability of possible thermal regimes of spheres in supersonic and hypersonic flows, the effect of the sphere temperature is studied via two limit simulations: cold sphere at $T_w = T_\infty$ and hot sphere $T_w = T_s$. In addition, the value $T_w = 1000$ K is considered. To consider the effects of surface state for various gaseous species, several sets of the accommodation coefficients α_t and α_n are used in the calculations.

To relate the input dimensionless parameters Ma and δ to conditions in a real flow, the gas viscosity and its atomic mass are required. To this end, the most precise values of the viscosity obtained for the AI potentials by Cencek *et al.* (2012) and Sharipov & Benites (2017, 2019, 2020) are used here for helium, neon, argon and krypton. As is known, the noble gases are never pure, but are composed of several isotopes (Meija *et al.* 2016). The consideration of an isotope mixture as a single gas can also affect all characteristics of the flow. The calculations of viscosity and thermal conductivity for isotope mixtures of neon, argon and krypton by Sharipov & Benites (2021) pointed out that the effect of the isotope composition on the transport coefficients does not exceed 0.01 %, which is much smaller than the numerical error of the calculations reported in the present paper. Thus neon, argon and krypton are considered as single gases, with average atomic masses using the composition reported by Meija *et al.* (2016) and atomic masses of each isotope provided by Wang *et al.* (2017). The isotopes ^{3}He and ^{4}He are considered as pure gases with the corresponding atomic masses. The values of viscosity μ at temperature 300 K and atomic masses used here are summarized in table 1.

The quantities of interest can be expressed in terms of the normal stress p_n, shear stress τ, and energy flux J_e to the sphere surface calculated via the distribution function $f = f(\boldsymbol{r}, \boldsymbol{v})$ as

$$p_n = \int m v_n^2 f \, \mathrm{d}\boldsymbol{v}, \quad \tau = \int m v_n v_t f \, \mathrm{d}\boldsymbol{v}, \quad J_e = \int \frac{1}{2} m |\boldsymbol{v}|^2 v_n f \, \mathrm{d}\boldsymbol{v}, \tag{2.8a–c}$$

where v_n and v_t are the components of the velocity $\boldsymbol{v}$ shown in figure 1. Since the flow is axisymmetric, the quantities defined on the sphere surface (2.8a–c) depend only on the angle θ shown in figure 1, and are independent of the azimuthal angle. The quantities p_n, τ and J_e are related to the pressure C_p, friction C_f, and energy transfer C_h coefficients:

$$C_p = \frac{p_n - p_\infty}{\rho_\infty U_\infty^2 / 2} = \frac{p_n - p_\infty}{p_\infty S^2}, \tag{2.9}$$

$$C_f = \frac{-\tau}{\rho_\infty U_\infty^2 / 2} = \frac{-\tau}{p_\infty S^2}, \tag{2.10}$$

$$C_h = \frac{-J_e}{\rho_\infty U_\infty^3 / 2} = \frac{-J_e}{p_\infty v_\infty S^3}. \tag{2.11}$$

Here, S is the speed ratio:

$$S = \frac{U_\infty}{v_\infty} = \sqrt{\frac{5}{6}} \, Ma. \tag{2.12}$$

The drag force F exerted on the sphere is given as

$$F = 2\pi R^2 \int_0^\pi (p_n \cos\theta - \tau \sin\theta) \sin\theta \, d\theta. \tag{2.13}$$

The drag coefficient C_D is expressed in terms of the drag force F as

$$C_D = \frac{F}{(\pi/2)R^2 \rho_\infty U_\infty^2} = \frac{F}{\pi R^2 p_\infty S^2}, \tag{2.14}$$

which can also be rewritten in terms of C_p and C_f as

$$C_D = 2 \int_0^\pi \left(C_p \cos\theta + C_f \sin\theta \right) \sin\theta \, d\theta. \tag{2.15}$$

The average energy transferred to the sphere is defined via C_h as

$$C_Q = \frac{1}{2} \int_0^\pi C_h \sin\theta \, d\theta. \tag{2.16}$$

The local characteristics of interest, namely, number density $n(\boldsymbol{r})$, temperature $T(\boldsymbol{r})$ and bulk velocity $\boldsymbol{u}(\boldsymbol{r})$, are defined via the distribution function $f = f(\boldsymbol{r}, \boldsymbol{v})$ as

$$n = \int f \, d\boldsymbol{v}, \quad \boldsymbol{u} = \frac{1}{n} \int \boldsymbol{v} f \, d\boldsymbol{v}, \quad T = \frac{m}{3nk_B} \int (\boldsymbol{v} - \boldsymbol{u})^2 f \, d\boldsymbol{v}. \tag{2.17a–c}$$

3. Gas–surface interaction

To solve the problem in terms of the velocity distribution function $f(\boldsymbol{r}, \boldsymbol{v})$, the boundary conditions have to be imposed on the sphere surface. The distribution function $f(\boldsymbol{r}, \boldsymbol{v})$ of the particles reflected from the surface is related to that of incident particles $f(\boldsymbol{r}, \boldsymbol{v}')$ as

$$v_n f(\boldsymbol{r}, \boldsymbol{v}) = - \int_{v_n' < 0} v_n' R(\boldsymbol{v}, \boldsymbol{v}') f(\boldsymbol{r}, \boldsymbol{v}') \, d\boldsymbol{v}', \quad v_n > 0, \tag{3.1}$$

where $R(\boldsymbol{v}, \boldsymbol{v}')$ is the scattering kernel. As was pointed out previously by Sharipov (2003a,b, 2016) and Kalempa & Sharipov (2020, 2021), the widely used diffuse–specular

model of gas–surface interaction is not consistent from the physical viewpoint. In fact, it contains only one parameter, which varies significantly when extracted from different experiments. The kernel proposed by Cercignani & Lampis ([1971](#)) contains two accommodation coefficients, namely, TMAC α_t and NEAC α_n. Moreover, it was derived by Cercignani ([1972](#)) using a physical model of solid surface based on the Fokker–Planck equation. Thus the CL kernel given as

$$R(\boldsymbol{v}', \boldsymbol{v}) = \frac{v_n}{\pi^2 \alpha_n \alpha_t (2 - \alpha_t) v_w^4} \exp\left[-\frac{(\boldsymbol{v}_t - (1 - \alpha_t)\boldsymbol{v}_t')^2}{\alpha_t(2 - \alpha_t)v_w^2} - \frac{v_n^2 + (1 - \alpha_n)v_n'^2}{\alpha_n v_w^2} \right]$$
$$\times \int_0^{2\pi} \exp\left(\frac{2\sqrt{1 - \alpha_n}\, v_n v_n' \cos\phi}{\alpha_n v_w^2} \right) \mathrm{d}\phi \tag{3.2}$$

is used in the present work. Here, $v_w = \sqrt{2k_B T_w/m}$ is the most probable speed at the surface temperature. In the particular case when $\alpha_n = 1$ and $\alpha_t = 1$, the kernel ([3.2](#)) corresponds to the model of diffuse scattering.

The typical values of the accommodation coefficients α_t and α_n published previously by Sharipov ([2003*a*,*b*](#)), Sharipov & Bertoldo ([2006](#)) and Sharipov & Moldover ([2016](#)) were extracted from experiments on Poiseuille flow reported by Porodnov *et al.* ([1974](#)), thermal creep by Porodnov *et al.* ([1978](#)), energy transfer between two cylinders by Semyonov *et al.* ([1984](#)), and energy transfer between two parallel plates by Trott *et al.* ([2011](#)). The coefficients α_t and α_n depend on gas species, and solid surface material and its state. According to Sharipov & Moldover ([2016](#)), the TMAC varies in the range $0.4 \leq \alpha_t \leq 1$, while the NEAC varies practically in the whole range, i.e. $0.01 \leq \alpha_n \leq 1$. The main trend is that the heavy gases, such as krypton, have accommodation coefficients close to 1, i.e. they are reflected diffusely from any surface. The light gases, such as helium and neon, have small accommodation coefficients for polished and clean surfaces. For instance, Sharipov & Moldover ([2016](#)) extracted $\alpha_t = 0.4$ and $\alpha_n = 0.01$ using the experimental data reported by Trott *et al.* ([2011](#)) for helium interacting with an aluminium surface treated by plasma. Using the same data for argon, the values $\alpha_t = 0.9$ and $\alpha_n = 0.85$ were obtained. Analysing the experimental data by Porodnov *et al.* ([1974](#), [1978](#)) and Semyonov *et al.* ([1984](#)) for helium interacting with a non-treated surface, the values $\alpha_t = 0.9$ and $\alpha_n = 0.1$ were extracted by Sharipov ([2003*a*,*b*](#)) and Sharipov & Bertoldo ([2006](#)). Thus to consider various surface types, the calculations are performed for all gases at diffuse reflection ($\alpha_t = 1$ and $\alpha_n = 1$), for argon assuming $\alpha_t = 0.9$ and $\alpha_n = 0.85$, and for helium using two sets of accommodation coefficients: (i) $\alpha_t = 0.4$ and $\alpha_n = 0.01$; (ii) $\alpha_t = 0.9$ and $\alpha_n = 0.1$. In accordance with the experimental data, only the sets of accommodation coefficients where $a_t > a_n$ are considered here.

4. Free molecular flow regime

The approach for calculation of aerothermodynamic coefficients of a body in a steady-state free molecular flow based on the diffuse–specular model of gas–surface interaction is well known (see e.g. Kogan [1969](#); Bird [1994](#)). The CL kernel was used by Chernyak & Sograbi ([2019](#)) and Kalempa & Sharipov ([2020](#)) to calculate the drag force in the case of low Mach numbers. In this section, the aerothermodynamic characteristics based on the CL kernel are calculated for arbitrary Mach number and temperature ratio T_w/T_∞.

In the collisionless limit ($\delta \to 0$), the distribution function of incident particles is given by the Maxwellian ([2.1](#)). The distribution function of reflected particles is obtained by

substituting (2.1) into the right-hand side of the boundary conditions (3.1). Then the local quantities (2.8a–c) are computed. They can be written in a compact form using the notation

$$\xi = S\cos\theta, \quad \eta = S\sin\theta, \tag{4.1a,b}$$

$$\Psi_1(S) = \frac{e^{-S^2}}{\sqrt{\pi}S}\left(1 + \frac{1}{2S^2}\right) + \left(1 + \frac{1}{S^2} - \frac{1}{4S^4}\right)\mathrm{erf}(S), \tag{4.2}$$

$$\Psi_2(S) = \frac{2e^{-S^2}}{\sqrt{\pi}S^3} + \left(\frac{2}{S^2} + \frac{1}{S^4}\right)\mathrm{erf}(S), \tag{4.3}$$

where $\mathrm{erf}(S)$ is the error function of S, and

$$\Phi(\alpha_n,\xi) = \frac{2}{\pi^{3/2}S^2\alpha_n(T_w/T_\infty)}\int_0^\infty\int_0^\infty\int_0^{2\pi}c^2c'$$
$$\times\exp\left(-\frac{c^2 + (1-\alpha_n)c'^2 - 2\sqrt{1-\alpha_n}\,cc'\cos\phi}{\alpha_n(T_w/T_\infty)} - (c'-\xi)^2\right)\mathrm{d}\phi\,\mathrm{d}c'\,\mathrm{d}c. \tag{4.4}$$

The last expression can be simplified in the limits $\alpha_n = 0$ and $\alpha_n = 1$ as

$$\Phi(0,\xi) = \frac{1}{S^2}\left[\left(\xi^2 + \frac{1}{2}\right)(1 + \mathrm{erf}(\xi)) + \frac{\xi e^{-\xi^2}}{\sqrt{\pi}}\right], \tag{4.5}$$

$$\Phi(1,\xi) = \frac{\sqrt{T_w/T_\infty}}{2S^2}\left[\sqrt{\pi}\xi(1 + \mathrm{erf}(\xi)) + e^{-\xi^2}\right]. \tag{4.6}$$

It can be verified that

$$\Phi(0,\xi) > \Phi(1,\xi) \quad \text{at } T_w/T_\infty = 1. \tag{4.7}$$

Then the pressure coefficient reads

$$C_p = \frac{1}{S^2}\left[\left(\xi^2 + \frac{1}{2}\right)(1 + \mathrm{erf}(\xi)) + \frac{\xi e^{-\xi^2}}{\sqrt{\pi}} - 1\right] + \Phi(\alpha_n,\xi), \tag{4.8}$$

where the terms in the square brackets correspond to the contribution of incident particles and depend only on the speed ratio S and the angle θ. The last term, Φ, in (4.8) corresponds to the reflected particles and depends on NEAC α_n, speed ratio S, temperature ratio T_w/T_∞, and angle θ, but it is independent of TMAC α_t. The inequality (4.7) points out that the coefficient C_p increases with decreasing NEAC α_n when $T_w/T_\infty = 1$.

The local friction coefficient can be expressed as

$$C_f = \frac{\alpha_t\eta}{S^2}\left[\xi(1 + \mathrm{erf}(\xi)) + \frac{e^{-\xi^2}}{\sqrt{\pi}}\right]. \tag{4.9}$$

As expected, it is proportional to TMAC α_t but is independent of NEAC α_n and temperature ratio T_w/T_∞.

The drag coefficient C_D is obtained substituting (4.8) and (4.9) into (2.15):

$$C_D = (1 + \alpha_t)\Psi_1(S) + \frac{2}{S^2}\int_{-S}^S\xi\,\Phi(\alpha_n,\xi)\,\mathrm{d}\xi. \tag{4.10}$$

The first term on the right-hand side of this equation depends only on TMAC α_t. It is largest for the diffuse reflection ($\alpha_t = 1$), and decreases with decreasing TMAC.

α_t	α_n	C_D at $T_w = T_\infty$				C_D at $T_w = T_s$			
		$Ma = 1$	2	5	10	$Ma = 1$	2	5	10
0.4	0.01	4.573	3.061	2.509	2.410	4.574	3.063	2.511	2.395
0.4	0.1	4.519	3.014	2.463	2.360	4.532	3.033	2.484	2.315
0.4	0.3	4.400	2.905	2.351	2.250	4.444	2.970	2.425	2.213
0.9	0.1	5.473	3.653	2.986	2.866	5.486	3.672	3.007	2.821
0.9	0.5	5.233	3.426	2.748	2.629	5.315	3.550	2.895	2.656
0.9	0.85	5.015	3.191	2.450	2.321	5.176	3.454	2.812	2.596
1.0	1.0	5.110	3.202	2.354	2.152	5.310	3.544	2.886	2.686

Table 2. Drag coefficient C_D versus accommodation coefficients α_t and α_n in free molecular flow at $T_w = T_\infty$ and $T_w = T_s$ according to (4.10).

The second term in (4.10) given by the four-fold integral depends on α_n, T_w/T_∞ and S via (4.4). Since the function $\Phi(\alpha_n, \xi)$ increases with decreasing NEAC α_n at $T_w/T_\infty = 1$, the drag coefficient increases as well when α_n decreases.

The local energy transfer coefficient is equal to

$$C_h = \frac{1}{2S^3} \left\{ \left[\frac{e^{-\xi^2}}{\sqrt{\pi}} + \xi(1 + \mathrm{erf}(\xi)) \right] \left[\alpha_n \left(\xi^2 + \frac{3}{2} - \frac{T_w}{T_\infty} \right) \right. \right.$$
$$\left. \left. + \alpha_t(2 - \alpha_t) \left(\eta^2 + 1 - \frac{T_w}{T_\infty} \right) \right] - \frac{\alpha_n e^{-\xi^2}}{2\sqrt{\pi}} \right\}, \tag{4.11}$$

so it depends on both α_t and α_n. The average energy transfer coefficient can be derived by inserting (4.11) into (2.16):

$$C_Q = \frac{1}{8} \left[\alpha_n + \alpha_t(2 - \alpha_t) \right] \left[\Psi_1(S) + \left(1 - \frac{T_w}{T_\infty} \right) \Psi_2(S) \right], \tag{4.12}$$

where Ψ_1 and Ψ_2, given by (4.2) and (4.3), are functions of the speed ratio S only. The expression (4.12) shows that the coefficient C_Q reaches its maximum value for diffuse reflection ($\alpha_t = 1$ and $\alpha_n = 1$) and decreases with decreasing either α_t or α_n.

The dependence (4.12) of the energy transfer coefficient C_Q on the accommodation coefficients and temperature ratio T_w/T_∞ is explicit and can be understood easily. In contrast, the drag coefficient (4.10) contains the four-fold integral, therefore its dependence on the NEAC and temperature ratio is not obvious. To reveal this dependence, the numerical values of C_D calculated via (4.10) are given in table 2 for some sets of α_t, α_n, and for two values of the temperature T_w: $T_w = T_\infty$ and $T_w = T_s$. The data show that the drag coefficient decreases with increasing NEAC. The effect of the ratio T_w/T_∞ on C_D depends on the NEAC: it is strongest at $\alpha_n = 1$, but it becomes very weak at $\alpha_n \leq 0.5$.

5. Method of solution in the transitional flow regime

5.1. *Computational domain and boundary conditions*

The flow under consideration is axisymmetric so that the computational domain represents a cylinder of radius R_d and length $2R_d$, with the sphere placed in its centre as shown in figure 2. According to the DSMC method (Bird 1994, 2013), the domain is divided into a
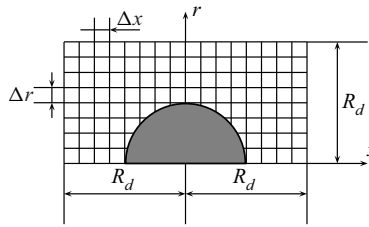
Figure 2. Scheme of computational domain.

regular mesh of cells with sizes Δr and Δx in the radial and axial directions, respectively. For the sake of simplicity, we consider $\Delta x = \Delta r$. The positions (r, x) of all modelling particles, and three components of their velocities $\boldsymbol{v}$, are stored in computer memory. The time is also discretized and advanced by a step Δt. Then the following procedures are realized. (i) The free motion of modelling particles during the time interval Δt is simulated. Since only the radial and axial coordinates for modelling particles are saved, the azimuthal component of the velocity must be changed to compensate the azimuthal displacement of each particle. (ii) The binary interatomic collisions in accordance with the number of particles and their velocities in each cell are simulated by computing new molecular velocities. (iii) Calculations of macroscopic quantities such as the local density n, temperature T and bulk (or gas) velocity $\boldsymbol{u}$ are performed.

To provide a more uniform distribution of modelling particles over the radial direction, a weight depending on the radial coordinate r is attributed to each particle. When particles move from the x-axis to the periphery, some of them are randomly eliminated, and the weights of remaining particles are increased. If particles move from the periphery to the x-axis, then their weights are decreased and new particles are generated.

During the free motion step, some particles collide with the sphere surface. In this case, their new velocities are generated according to the CL scattering kernel (3.2). The procedure to generate velocities of reflected particles is described by Lord (1991) and Sharipov (2016). Some particles leave the domain during free motion, and the information about them is removed. Simultaneously, new particles are generated at the domain boundaries following the procedure described in § 4.1 of the book by Bird (2013), based on the free stream distribution functions (2.1). Details of the approach utilized in this work to generate new particles are provided in the supplementary material.

5.2. *Intermolecular collisions*

The numerical scheme by Sharipov (2018*b*) to simulate interatomic collisions based on AI potentials does not depend on the flow type. Here, we use the same scheme that was developed previously for simulations of shock waves (Sharipov & Dias 2019; Dias & Sharipov 2021) and energy and momentum transfer between two plates (Ambrus, Sharipov & Sofonea 2020). During an elastic collision, the relative velocity $\boldsymbol{g}$ changes its direction, keeping the magnitude. A calculation of the angle between relative velocities before and after a collision, i.e. the deflection angle χ, requires significant computational effort. The main idea of the scheme proposed by Sharipov (2018*b*) is to calculate the lookup tables (scattering matrices) of the deflection angle. First, the differential cross-section (DCS) and total cross-section (TCS) are calculated for many values of the relative speed $g = |\boldsymbol{g}|$ using a quantum approach. Then a fixed number of deflection angles is calculated in the interval $[0, \pi/2]$ such that these discrete angles become equiprobable. In other words, the nodes

of the angle mesh are denser in a region corresponding to a larger DCS. The scattering matrices for helium and neon are given in the supplementary material to the paper by Sharipov & Dias (2019), and those for argon and krypton are given in the supplementary material to the paper by Dias & Sharipov (2021). All of them have the same structure, i.e. 900 values of the relative speed g, and 100 values of the deflection angles χ. The tables also contain the TCS for each value of g_j. If a randomly chosen pair of modelling particles has a relative speed g, then the index j is calculated as

$$j = \left\lfloor \frac{\ln(1 + g/G)}{\ln 1.005} + \frac{1}{2} \right\rfloor, \quad 1 \le j \le 900, \tag{5.1}$$

where G depends on the gas species and is given in table 1. Then the pair undergoes the rejection–acceptance collision test using the corresponding values of the TCS. If the collision between the considered pair of particles is accepted, then the index i is chosen randomly from the range $1 \le i \le 100$. The element ξ_{ij} taken from the scattering matrix is used as $\cos \chi$ to calculate the post-collision velocities according to (8.32)–(8.35) from the book by Sharipov (2016).

As is known, the simplest model of the interatomic interaction, namely the HS model, does not provide a correct dependence of viscosity on gas temperature. However, it is still used widely because of some advantages such as the simplicity of its implementation and non-necessity to specify the gas species. In addition, the results of aerodynamic calculations based on the HS model can be presented in a dimensionless form that does not explicitly depend on the dimensional temperature of the free stream. Therefore, it is important to know the uncertainty of the HS model that depends on the flow type and on the input parameters determining the solution. To this end, the calculations are also performed for the HS model.

5.3. *Calculation of macroscopic quantities*

The approach to calculations of the macroscopic properties is described in § 8.6 of the book by Sharipov (2016) and in some papers (e.g. Sharipov 2017; Sharipov & Dias 2017). For the problem in question, the number density n, temperature T and bulk velocity $\boldsymbol{u}$ defined by (2.17a–c) are calculated following that standard procedure.

The contribution of each individual modelling particle to the stress and energy flux defined by (2.8a–c) is accounted for when the straight particle trajectory crosses the sphere surface. The corresponding procedure described below does not involve any additional approximation. The moments of the distribution function on the sphere surface (2.8a–c) are calculated via the differences of the corresponding properties between the reflected and incident fluxes. First, the angle θ shown in figure 1 is discretized as $\theta_j = (j - 0.5)\,\Delta\theta$ ($1 \le j \le N_\theta$), where $\Delta\theta = \pi/N_\theta$, and N_θ is an integer number of surface cells. Then the incident $\boldsymbol{v}_i^{inc}$ and reflected $\boldsymbol{v}_i^{ref}$ velocities are registered for the ith particle interacting with the surface element of area $\Delta A_j = \pi R^2 \left[\cos(\theta_j - \Delta\theta/2) - \cos(\theta_i + \Delta\theta/2)\right]$. Finally, the surface moments (2.8a–c) are calculated for each surface element as

$$\begin{bmatrix} p_n(\theta_j) \\ \tau(\theta_j) \\ J_e(\theta_j) \end{bmatrix} = \frac{m}{N_s\,\Delta t\,\Delta A_j} \sum_{i=1}^{N_j} W_i \begin{bmatrix} v_{ni}^{ref} + v_{ni}^{inc} \\ v_{ti}^{ref} - v_{ti}^{inc} \\ \left(|v^{ref}|^2 - |v^{inc}|^2\right)/2 \end{bmatrix}, \tag{5.2}$$

where W_i is the weighting factor, i.e. the number of real particles represented by the ith model particle, v_{ni} is the normal component of velocity of the ith particle, and v_{ti} is its

	R_d/R				$R/\Delta r$			
δ	$Ma = 1$	2	5	10	$Ma = 1$	2	5	10
0.1	8	8	8	6	20	20	20	20
1	12	8	4	3	20	20	40	40
10	20	4	4	3	60	60	80	160
30	30	4	3	3	80	80	120	240

Table 3. Parameters of the numerical scheme.

tangential component, and N_j is the number of incident particles on the surface element ΔA_j during N_s time steps needed to calculate the macroscopic quantities.

The drag force on the sphere in (2.13) is calculated via the difference of the momentum mv_x between the reflected and incident fluxes over the whole sphere surface, i.e.

$$F = \frac{m}{N_s \, \Delta t} \sum_{i=1}^{N_{tot}} W_i \left(v_{xi}^{ref} - v_{xi}^{inc} \right). \tag{5.3}$$

Here, N_{tot} is the total number of particles that hit the sphere during N_s time steps, and v_{xi} is the x-component of velocity of the ith particle hitting the sphere.

5.4. *Parameters of numerical scheme and accuracy*

In the problem under consideration, the numerical error is determined by the following numerical scheme parameters: size of the computational domain R_d, size of cells Δr, number of modelling particles per cell N_p in the free stream flow, time step Δt, number of time steps N_{steady} required to establish steady-state flow, and number of time steps N_s to calculate the macroscopic quantities. The values of these parameters were chosen to ensure that their further variations to improve the numerical accuracy do not change the drag coefficient C_D and the average energy transfer coefficient C_Q within 0.5 %.

The optimum value of each parameter depends on both Mach number Ma and rarefaction parameter δ. The size of the computational domain R_d and the cell size are given in table 3. The largest size $R_d = 30R$ corresponds to $Ma = 1$ and $\delta = 30$, while the smallest size $R_d = 3R$ is used at $Ma = 10$ and $\delta = 30$. The cell size varies from $\Delta r = R/240$ used at $Ma = 10$ and $\delta = 30$, to $\Delta r = R/20$ used at $\delta = 0.1$ for all values of Ma. The number of modelling particles is not smaller than $N_p = 50$ in all cases. The time step varies from $\Delta t = 0.002R/v_\infty$ at $\delta = 30$ to $\Delta t = 0.005R/v_\infty$ at $\delta = 0.1$. Finally, the number of samples to compute the aerothermodynamic characteristics varies from $N_s = 10^4$ at $Ma = 10$ to 10^5 at $Ma = 1$, while the number of time steps to establish the steady-state flow is $N_{steady} = N_s/10$.

Some examples of influence of the parameters R_d, Δr and Δt on C_D and C_Q are given in the supplementary material, showing the convergence of the coefficients C_D and C_Q when R_d increases or when Δr and Δt decrease. The statistical scattering of C_D and C_Q estimated via their standard deviations over N_s time steps was smaller than 0.1 %. The procedures to estimate the statistical scattering and characteristic values of the standard deviation are provided in the supplementary material. It was found that the results do not change within the statistical scattering when a double number of particles, i.e. $N_p = 100$, is considered.

The three steps of the DSMC method – namely, free motion, intermolecular collisions and calculation of macroscopic characteristics – are elaborated independently from each other so that they can be validated separately. Since the free motion of particles and calculation of the macroscopic characteristics are independent on the intermolecular collision procedure, they are validated in the free molecular regime ($\delta = 0$). The numerical values of C_D, C_Q, C_p, C_f and C_h obtained by the DSMC method with the numerical scheme parameters described above, and assuming $\delta = 0$, were compared with their analytical values given in § 4. It was verified that the disagreement is within 0.1 % for all values of TMAC α_t and NEAC α_n. The intermolecular collision procedure independent of the flow configuration was the same as that used in the previous papers Sharipov (2018*a*), Sharipov & Dias (2019), Zhu *et al.* (2019) and Dias & Sharipov (2021). It was validated previously via calculations of viscosity and thermal conductivity by the DSMC method (Sharipov & Strapasson 2012*b*) over a wide temperature range. As a result, the transport coefficients calculated by completely different methods (Cencek *et al.* 2012; Hellmann *et al.* 2008; Sharipov & Benites 2017, 2019, 2020) and measured with high accuracy (Berg & Burton 2013) were reproduced by the DSMC method within 0.1 %, which is smaller than the numerical error of the present results.

6. Results and discussion

6.1. *Effect of gas species*

First, the aerothermodynamic characteristics C_D and C_Q were calculated for the temperatures of the sphere T_w and free stream T_∞ equal to 300 K assuming diffuse scattering on the sphere surface for all considered gases, namely, helium (^{4}He), neon, argon and krypton. The corresponding data together with those for the HS model are presented in table 4. The coefficients C_D and C_Q for ^{3}He at $T_w = T_\infty = 300$ K are the same as those for ^{4}He within the numerical accuracy, so they are not reported in table 4.

As expected, the coefficients C_D and C_Q depend strongly on both *Ma* and δ. Their values for the HS model differ significantly from those for the AI potentials of all species at large values of the Mach number. In the case $Ma = 10$, the relative differences of C_D and C_Q based on the HS model from those for krypton are 10 % and 27 %, respectively. For $Ma = 1$, the relative differences become much smaller, namely, 1.3 % and 4.6 % for C_D and C_Q, respectively.

A comparison of C_D and C_Q for all species calculated based on the AI potentials shows that their values for neon are systematically smaller and those for krypton are always larger in comparison with the other gases. The relative deviations of C_D and C_Q for neon and krypton are plotted in figure 3. These differences at $Ma = 1$ do not exceed 1 % and 3 % for C_D and C_Q, respectively. At larger Mach numbers, the relative differences reach 3 % and 7 % for C_D and C_Q, respectively.

The fields of density n/n_∞, temperature T/T_∞, gas speed u/U_∞ ($u = |\boldsymbol{u}|$), and streamlines of neon at $Ma = 2$ are shown in figure 4 for two values of the rarefaction parameter, $\delta = 1$ and $\delta = 30$. These are typical flow fields in the transitional ($\delta = 1$) and hydrodynamic ($\delta = 30$) flow regimes. The former is characterized by the smooth variation of all quantities n/n_∞, T/T_∞, u/U_∞ and by the gas perturbed at a long distance from the sphere front surface. The latter is distinguished by the shock wave, where the macroscopic variables vary sharply from their values in the free stream to significantly different ones. In this case, a vortex arises just behind the sphere. The flow fields for other values of *Ma* are given in the supplementary material.

		C_D					C_Q				
Ma	δ	HS	^{4}He	Ne	Ar	Kr	HS	^{4}He	Ne	Ar	Kr
1	0.1	4.876	4.891	4.897	4.898	4.899	0.4497	0.4508	0.4523	0.4526	0.4529
	0.3	4.494	4.505	4.504	4.512	4.526	0.3994	0.4034	0.4027	0.4053	0.4086
	1	3.683	3.701	3.701	3.714	3.722	0.2909	0.2967	0.2970	0.3010	0.3040
	3	2.800	2.816	2.815	2.827	2.835	0.1757	0.1792	0.1790	0.1820	0.1839
	10	2.061	2.065	2.065	2.073	2.078	0.09339	0.09422	0.09415	0.09513	0.09550
	30	1.561	1.564	1.564	1.568	1.569	0.05524	0.05524	0.05507	0.05531	0.05553
2	0.1	2.998	3.017	3.013	3.022	3.034	0.2938	0.2964	0.2956	0.2972	0.2987
	0.3	2.725	2.763	2.760	2.780	2.794	0.2592	0.2636	0.2632	0.2660	0.2681
	1	2.278	2.322	2.317	2.345	2.360	0.1953	0.2019	0.2010	0.2054	0.2075
	3	1.850	1.882	1.879	1.901	1.915	0.1297	0.1342	0.1336	0.1368	0.1390
	10	1.531	1.545	1.544	1.554	1.561	0.07696	0.07922	0.07899	0.08069	0.08166
	30	1.331	1.337	1.336	1.341	1.345	0.04715	0.04851	0.04838	0.04925	0.04986
5	0.1	2.155	2.201	2.193	2.205	2.213	0.2352	0.2415	0.2404	0.2420	0.2431
	0.3	1.977	2.044	2.030	2.046	2.060	0.2085	0.2183	0.2164	0.2188	0.2208
	1	1.734	1.813	1.797	1.818	1.835	0.1649	0.1778	0.1754	0.1790	0.1818
	3	1.479	1.557	1.542	1.565	1.582	0.1159	0.1291	0.1265	0.1306	0.1338
	10	1.243	1.287	1.277	1.293	1.305	0.07150	0.07966	0.07800	0.08085	0.08304
	30	1.108	1.126	1.122	1.131	1.138	0.04500	0.04965	0.04863	0.05048	0.05185
10	0.1	1.953	2.026	2.012	2.018	2.024	0.2246	0.2351	0.2331	0.2341	0.2349
	0.3	1.833	1.922	1.903	1.911	1.918	0.2019	0.2171	0.2139	0.2155	0.2169
	1	1.659	1.779	1.751	1.762	1.773	0.1633	0.1856	0.1807	0.1832	0.1856
	3	1.417	1.565	1.530	1.548	1.564	0.1153	0.1415	0.1354	0.1389	0.1421
	10	1.179	1.281	1.253	1.269	1.283	0.07068	0.08916	0.08438	0.08725	0.08990
	30	1.055	1.103	1.090	1.099	1.107	0.04487	0.05589	0.05306	0.05490	0.05658

Table 4. Drag C_D and average energy transfer C_Q coefficients versus Mach number *Ma* and rarefaction parameter δ for diffuse scattering ($\alpha_t = 1$ and $\alpha_n = 1$) at $T_\infty = T_w = 300$ K.

6.2. *Effect of free stream temperature*

As is known, any dimensionless characteristics of rarefied gas obtained in term of the rarefaction parameter δ are independent of a reference temperature used in the definition (2.3) when the HS model is used. In fact, the viscosity based on this model is proportional to $T_\infty^{1/2}$, so the rarefaction parameter is proportional to the ratio p_∞/T_∞, i.e. the value of δ is determined only by the number density n_∞. The TCS used in the simulation of interatomic collisions is constant for the HS model. As a result, a dimensionless simulation based on the HS model does not require a specification of the gas reference temperature. The dependence of viscosity on the temperature based on the AI potentials (Cencek *et al.* 2012; Sharipov & Benites 2017, 2019, 2020) is different from that for the HS model and cannot be expressed by a simple formula like $\mu \propto T^\omega$. In this case, the rarefaction parameter is necessarily determined by two variables, p_∞ and T_∞, but not only by their ratio. Moreover, since a TCS based on the AI potentials depends on the relative velocity (Sharipov 2018b), the simulations performed for different temperatures use different values of the TCS. Therefore, a simulation can be performed when both δ and T_∞ are specified. It means that one can obtain different values of the aerothermodynamic characteristics by
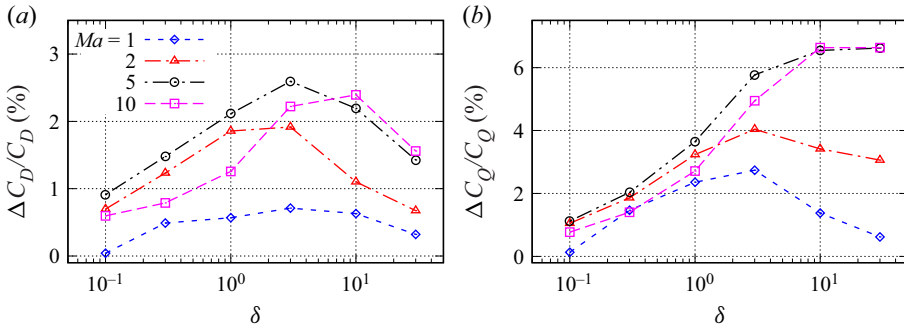
Figure 3. Relative deviations of coefficients (*a*) C_D and (*b*) C_Q for krypton from those for neon versus rarefaction parameter δ at diffuse scattering and $T_\infty = T_w = 300$ K. Here, $\Delta C_i/C_i = (C_i^{Kr} - C_i^{Ne})/C_i^{Ne}$, $i = D, Q$.

varying the temperature T_∞ at fixed δ, Ma and T_w/T_∞; i.e. the free stream temperature T_∞ affects the solution to the problem in question (Volkov & Sharipov 2017).

To reveal the effect of the free stream temperature T_∞ on the aerothermodynamic characteristics, the coefficients C_D and C_Q were calculated in a wide range of T_∞, assuming $T_w = T_\infty$. The corresponding results are plotted in figure 5 for the transitional flow regime at $\delta = 1$, and for two Mach numbers $Ma = 2$ and 5. The plots show that the values of C_D and C_Q are strongly sensitive to the free stream temperature T_∞. In fact, both coefficients C_D and C_Q for all gases except ^{3}He have maxima near the temperatures $T_\infty = 1.5$ K, 20 K, 90 K and 120 K for ^{4}He, Ne, Ar and Kr, respectively. The values of C_D and C_Q for ^{3}He gas have a minimum at $T_\infty = 1.5$ K. The relative variations of C_D and C_Q due the variation of the free stream temperature T_∞ are 8 % and 15 %, respectively. Such a dependence of the coefficients C_D and C_Q on T_∞ is similar to that of the shock wave slopes reported by Dias & Sharipov (2021) for the same gases. The significant differences of C_D and C_Q for ^{4}He from those for ^{3}He at low temperatures are explained by quantum effects. Both ^{4}He and ^{3}He have the same potential, but the former is boson, while the latter is fermion. As a results, their cross-sections are significantly different from each other (Sharipov 2018*b*), which leads to the different dependences of C_D and C_Q on T_∞ for these two gases.

In the cases $Ma = 1$ and 10, the behaviours of C_D and C_Q are qualitatively the same as those shown in figure 5.

6.3. *Effect of gas–surface interaction parameters*

As mentioned in §3, additional calculations were performed for helium-4 using two sets of TMAC and NEAC: (i) $\alpha_t = 0.4$ and $\alpha_n = 0.01$; (ii) $\alpha_t = 0.9$ and $\alpha_n = 0.1$. The former corresponds to a treated and polished metal surface, while the latter describes the interaction of helium with a non-treated surface. The third set, (iii) $\alpha_t = 0.9$ and $\alpha_n = 0.85$, considered here is specific for argon interacting with a treated metal surface.

The values of the aerothermodynamic coefficients C_D and C_Q for helium with sets (i) and (ii), and for argon with set (iii), are compared in figure 6 to those for argon interacting with the sphere surface diffusely. Note that when the diffuse interaction is assumed, the quantities C_D and C_Q of argon are very close to those of helium that are omitted in figure 6. The horizontal lines in these plots show the free molecular ($\delta = 0$) values of C_D and C_Q
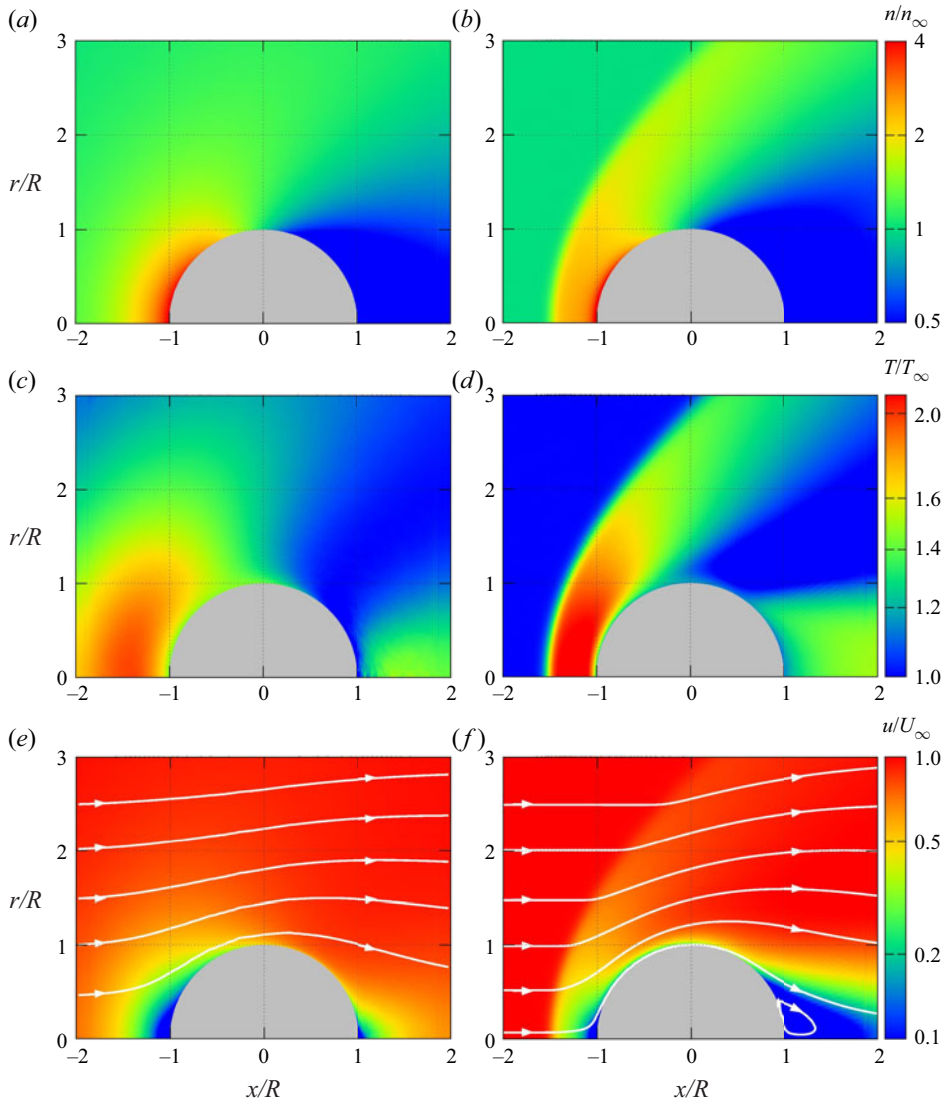
Figure 4. Fields of (*a*,*b*) density n/n_∞, (*c*,*d*) temperature T/T_∞, and (*e*,*f*) speed u/U_∞, and streamlines of neon at $Ma = 2$, diffuse scattering, $T_\infty = T_w = 300$ K: (*a*,*c*,*e*) $\delta = 1$; (*b*,*d*,*f*) $\delta = 30$.

given in table 2, which help us to understand the dependence of these coefficients on α_t and α_n. Both C_D and C_Q decrease with increasing rarefaction parameter δ when the Mach number and accommodation coefficients are fixed. Set (ii) leads to the largest values of the drag coefficient C_D for all Mach numbers considered here, while set (i) corresponds to the smallest C_D in all cases except $Ma = 5$ and $\delta < 3$. Set (iii) can both decrease and increase the drag in comparison to diffuse reflection. The reasons for this complex behaviour of C_D as a function of the accommodation coefficients can be understood using the theoretical equations for the free molecular flow regime. According to (4.10), the formula for the drag coefficient C_D includes two terms, where the first depends only on α_t and the second depends only on α_n. The first term is proportional to $(1 + \alpha_t)$ and decreases with decreasing TMAC α_t, while the second term increases by decreasing NEAC α_n in
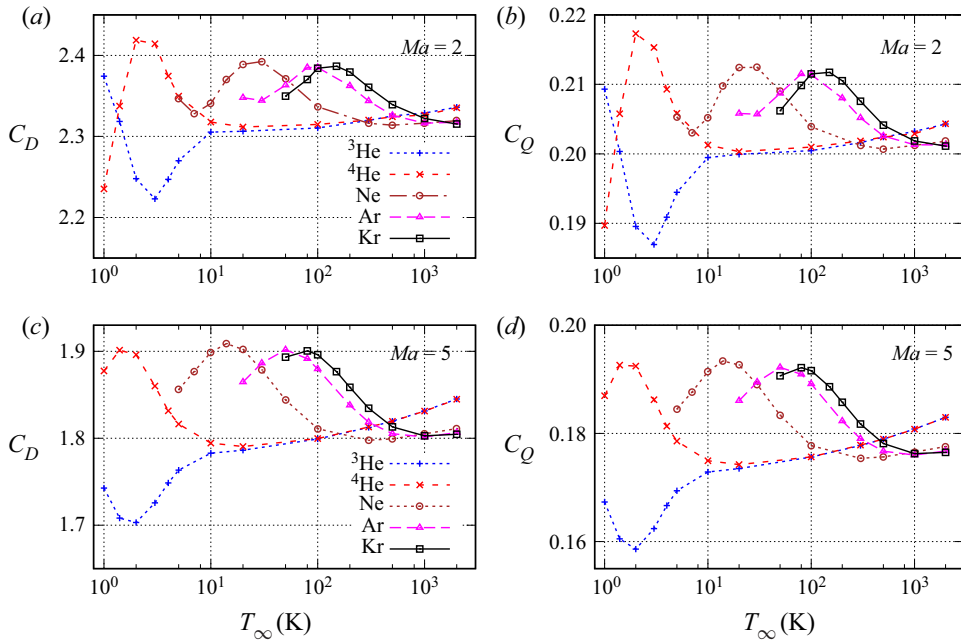
Figure 5. (*a,c*) Drag C_D and (*b,d*) average energy transfer C_Q coefficients versus free stream temperature T_∞ at $\delta = 1$, diffuse scattering, $T_w = T_\infty$.

accordance with the inequality (4.7). Both terms depend also on the speed ratio S. Thus the variation of coefficients α_t and α_n can both decrease and increase the drag coefficient depending on the Mach number. For instance, at $Ma = 5$ and $\delta = 0$, all considered sets of α_t and α_n lead to a larger drag coefficient compared to diffuse reflection. However, at $Ma = 1$ and $\delta = 0$, only set (ii) provides the drag coefficient that is larger than C_D at diffuse reflection, while the other two sets cause a reduction of the drag.

As expected, the energy transfer coefficient C_Q is largest for diffuse reflection. This coefficient always decreases with decreasing either TMAC α_t or NEAC α_n. The expression (4.12) shows that the coefficient C_Q in the free molecular flow regime is proportional to $[\alpha_n + \alpha_t(2 - \alpha_t)]$, which explains the largest value of C_Q at diffuse reflection. The effect of the gas–surface interaction model becomes weaker when the rarefaction parameter δ increases.

The axial distributions of the density n/n_∞, temperature T/T_∞ and gas velocity u_x/U_∞ along the stagnation streamline ($x < -R$) at $Ma = 1$ and 2 are depicted in figure 7. To demonstrate the effect of the gas–surface interaction parameters, the distributions of ^{4}He interacting with the sphere surface diffusely are compared to those of the same gas with the accommodation coefficients $\alpha_t = 0.4$ and $\alpha_n = 0.01$ corresponding to a treated surface. In the case $Ma = 1$, the density and temperature distributions are affected weakly by the rarefaction parameter δ and strongly by the gas–surface interaction parameters. The gas velocity u_x/U_∞ changes weakly with both rarefaction parameter δ and accommodation coefficients α_t and α_n. The distributions demonstrate the same behaviours in the case $Ma = 2$ and $\delta \leq 1$. However, they are completely different at $Ma = 2$ and $\delta = 30$, when the quantities n/n_∞, T/T_∞ and u_x/U_∞ change sharply at the point $x/R = -1.5$ corresponding to the shock wave position. In this case, the accommodation coefficients α_t and α_n
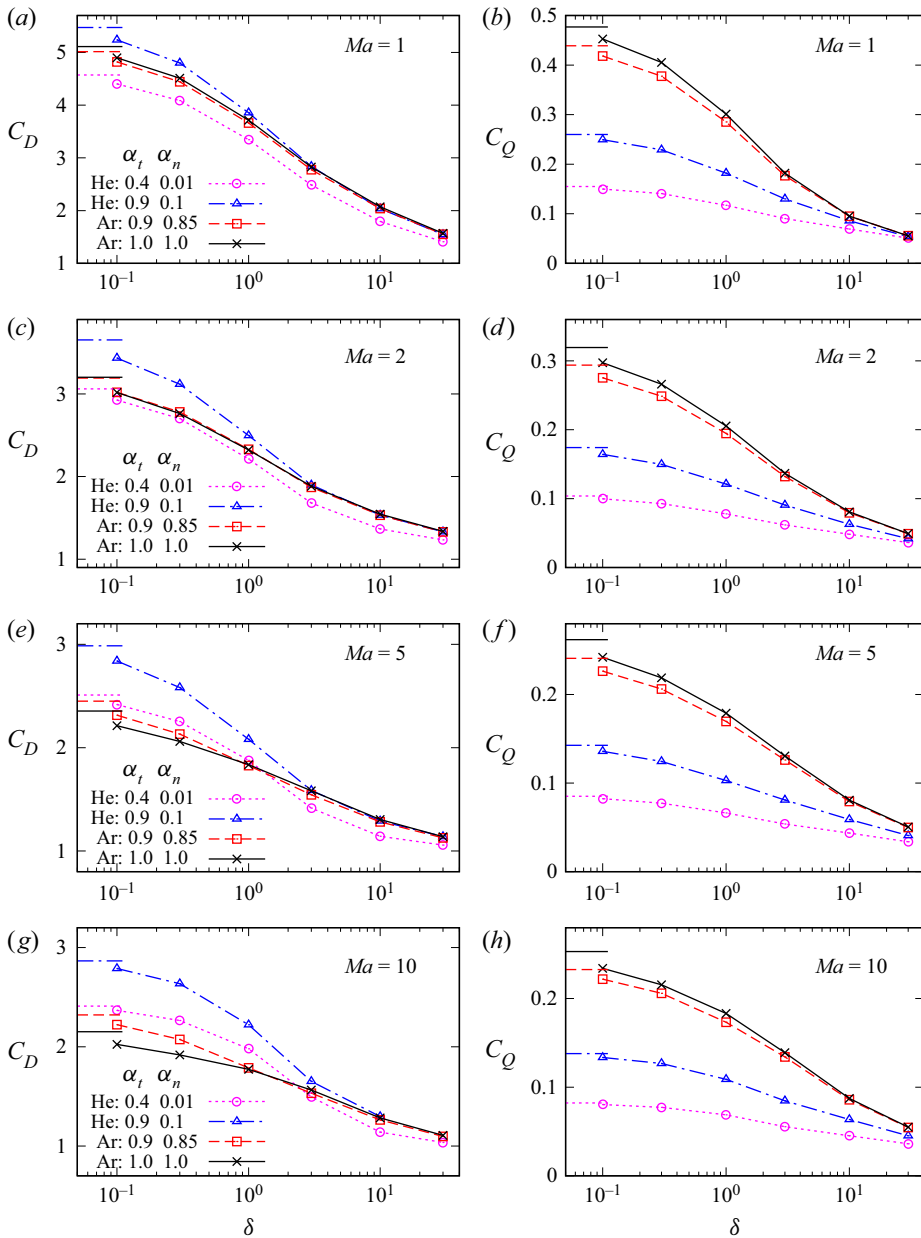
942 A17-20

Figure 6. (a,c,e,g) Drag C_D and (b,d,f,h) average energy transfer C_Q coefficients versus rarefaction parameter δ at $T_\infty = T_w = 300$ K for different sets of the accommodation coefficients α_t and α_n. The horizontal lines represent the free molecular limits given by (4.10) and (4.12).

practically do not affect the flow field. The profiles at $Ma = 5$ and 10 similar to those for $Ma = 2$ are given in the supplementary material.

The local pressure C_p, friction C_f, and energy transfer C_h coefficients for ^{4}He at the diffuse interaction ($\alpha_t = 1$ and $\alpha_n = 1$), and those for the set $\alpha_t = 0.4$ and $\alpha_n = 0.01$, are plotted against angle θ in figure 8. All these coefficients are sensitive to the accommodation coefficients, rarefaction parameter and Mach number. The pressure C_p
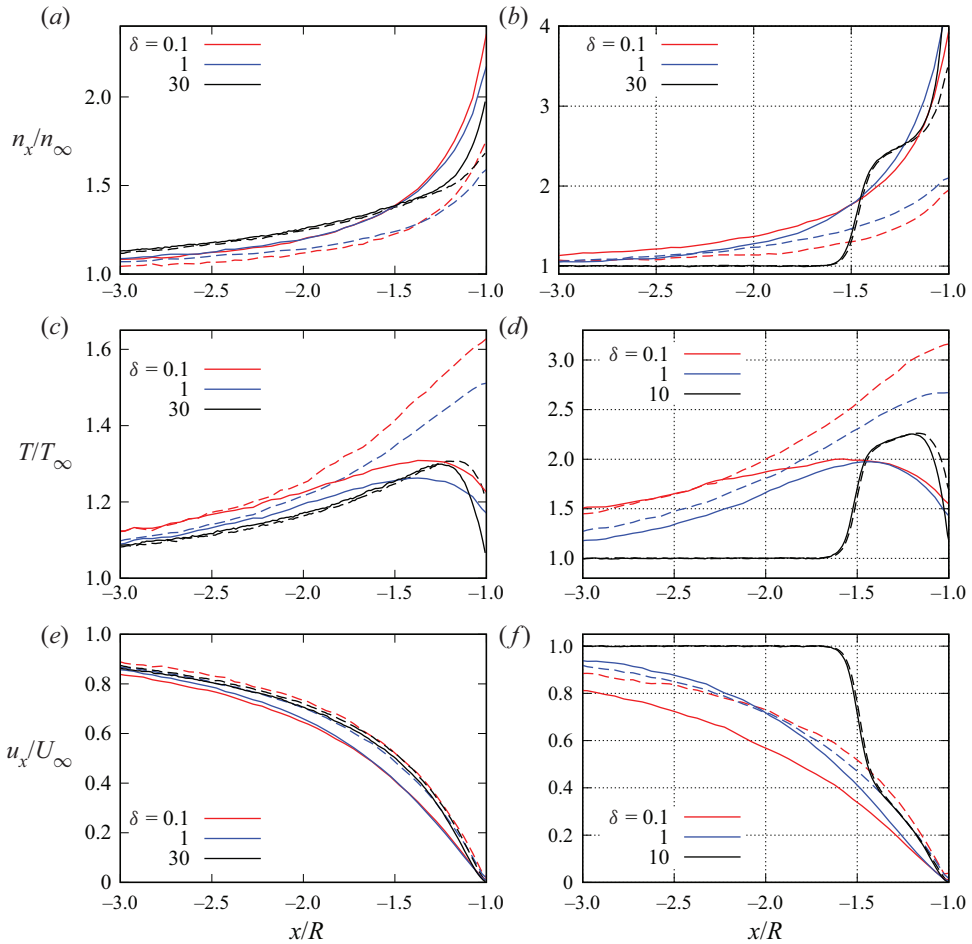
Figure 7. Axial distributions of (a,b) density n/n_∞, (c,d) temperature T/T_∞, and (e,f) velocity u_x/U_∞ at $T_\infty = T_w = 300$ K for ^{4}He: (a,c,e) $Ma = 1$; (b,d,f) $Ma = 2$. Solid lines indicate diffuse reflection; dashed lines indicate $\alpha_t = 0.4$, $\alpha_n = 0.01$.

and friction C_f coefficients have the same qualitative behaviours as functions of θ for all values of δ, Ma, α_t and α_n, while the energy transfer coefficient C_h differs qualitatively for diffuse ($\alpha_t = 1$, $\alpha_n = 1$) and non-diffuse ($\alpha_t = 0.4$, $\alpha_n = 0.01$) reflection. Curiously, the coefficient C_h has a minimum at the stagnation point $\theta = 0$ when $\delta \leq 1$.

6.4. *Effect of the sphere temperature*

To reveal the effect of T_w on the aerothermodynamic characteristics, the calculations at $T_w = T_s$ and $T_\infty = 300$ K were performed for ^{4}He interacting diffusely with the sphere surface. In addition, the fixed value $T_w = 1000$ K was considered for all Mach numbers, keeping $T_\infty = 300$ K. In the cases $Ma = 1$ and 2, the temperature $T_w = 1000$ K is higher than T_s. This can happen when the spherical particles immersed in a gas are heated by laser radiation. In the cases $Ma = 5$ and 10, the the temperature $T_w = 1000$ K lies in between T_∞ and T_s.
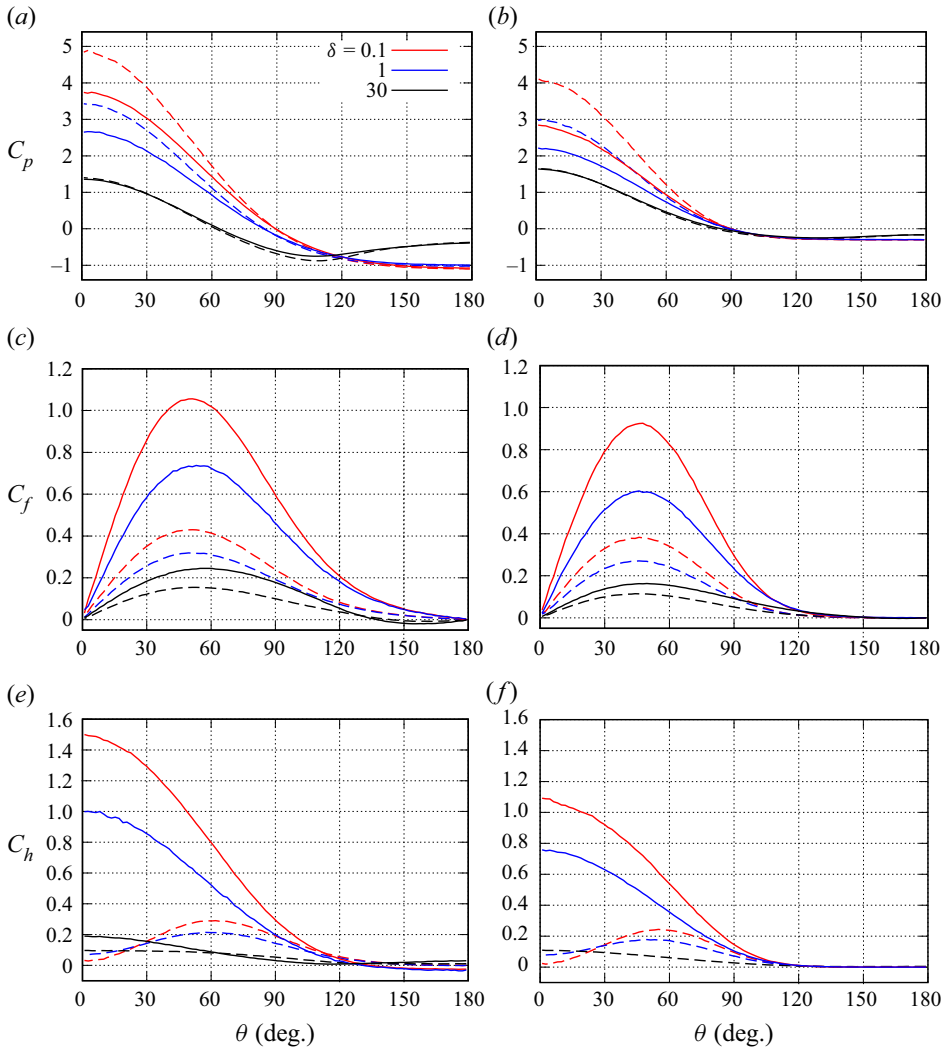
942 A17-22

Figure 8. (*a,b*) Pressure C_p, (*c,d*) friction C_f, and (*e,f*) energy transfer C_h coefficients versus angle θ at $T_\infty = T_w = 300$ K for ^{4}He: (*a,c,e*) $Ma = 1$; (*b,d,f*) $Ma = 2$. Solid lines indicate diffuse reflection; dashed lines indicate $\alpha_t = 0.4$, $\alpha_n = 0.01$.

The values of C_D and C_Q for these two values of the sphere temperature T_w are given in table 5. In the case $T_w = 1000$ K, the drag coefficient is strongly affected by T_w at $Ma = 1$, while the effect of T_w on C_D is weak at $Ma = 5$ and 10. This effect decreases with increasing the rarefaction parameter δ for a fixed Mach number. If $T_w = T_s$, then the drag coefficient at $Ma = 10$ and $\delta = 0.1$ increases 32 % in comparison with the cold sphere ($T_w = T_\infty$) at the same Ma and δ. The difference is smaller for the smaller Mach number and becomes 4 % at $Ma = 1$ and $\delta = 0.1$. For a fixed Mach number, the influence of T_w on the drag coefficient decreases drastically when the rarefaction parameter δ varies from 0.1 to 30. For instance, in the case $Ma = 10$ and $\delta = 30$, the increase of C_D is approximately 8 % when the temperature T_w varies from T_∞ to T_s. According to table 2, the influence of T_w on C_D in the free molecular regime ($\delta = 0$) becomes weaker when the NEAC α_n

Ma	δ	C_D		$C_Q \times 10^2$	
		$T_w = 1000\,\text{K}$	$T_w = T_s$	$T_w = 1000\,\text{K}$	$T_w = T_s$
1	0.1	5.925	5.083	−164.2	15.26
	0.3	5.421	4.677	−152.8	12.74
	1	4.270	3.802	−125.9	6.920
	3	3.046	2.852	−93.03	0.8720
	10	2.166	2.083	−63.47	−2.017
	30	1.690	1.590	−43.78	−1.815
2	0.1	3.534	3.353	−8.243	8.034
	0.3	3.221	3.051	−8.334	6.587
	1	2.604	2.493	−8.491	3.593
	3	1.954	1.921	−8.083	0.702
	10	1.575	1.565	−6.345	−0.522
	30	1.393	1.376	−4.600	−0.665
5	0.1	2.422	2.741	18.97	5.071
	0.3	2.224	2.516	16.87	4.049
	1	1.896	2.089	13.10	2.088
	3	1.568	1.617	8.914	0.187
	10	1.303	1.318	5.379	−0.483
	30	1.156	1.194	3.381	−0.431
10	0.1	2.144	2.685	22.42	4.737
	0.3	2.015	2.540	20.62	4.052
	1	1.807	2.193	17.24	2.412
	3	1.572	1.698	12.97	0.414
	10	1.295	1.324	8.176	−0.528
	30	1.119	1.186	5.148	−0.453

Table 5. Drag C_D and average energy transfer C_Q coefficients for ^{4}He versus Mach number *Ma* and rarefaction parameter δ at diffuse reflection ($\alpha_t = 1$ and $\alpha_n = 1$).

changes from 1 to 0.5. Thus the effect of T_w on C_D is insignificant for all Mach numbers and rarefaction parameters when $\alpha_n \leq 0.5$.

The average energy transfer coefficient C_Q is strongly sensitive to the sphere temperature T_w. It changes its sign at *Ma* = 1 and 2 for all δ when $T_w = 1000$ K, and at $\delta \geq 10$ for all *Ma* when $T_w = T_s$. The decrease of C_Q with increasing surface temperature is also predicted in the free molecular flow regime by (4.12).

The local friction coefficient C_f is not sensitive to the surface temperature T_w, so it is not analysed here. Note that in the free molecular flow regime, the coefficient C_f is completely independent of T_w, in accordance with (4.9). The expression (4.8) for the local pressure coefficient C_p at $\delta = 0$ points out its dependence on the surface temperature T_w via the term Φ given by (4.4). The local energy transfer coefficient C_h is also affected by T_w at $\delta = 0$ according to (4.12). The coefficients C_p and C_h for ^{4}He interacting diffusely with the sphere surface are plotted against angle θ in figure 9; the solid lines correspond to $T_w = 300$ K, and the dashed lines correspond to $T_w = T_s$. The pressure coefficient C_p is weakly sensitive to the surface temperature T_w in the hydrodynamic flow regime at $\delta = 30$, while it is strongly sensitive at $\delta = 0.1$ and 1 for all Mach numbers. The energy transfer coefficient C_h is strongly sensitive to T_w for all values of the rarefaction parameter δ for
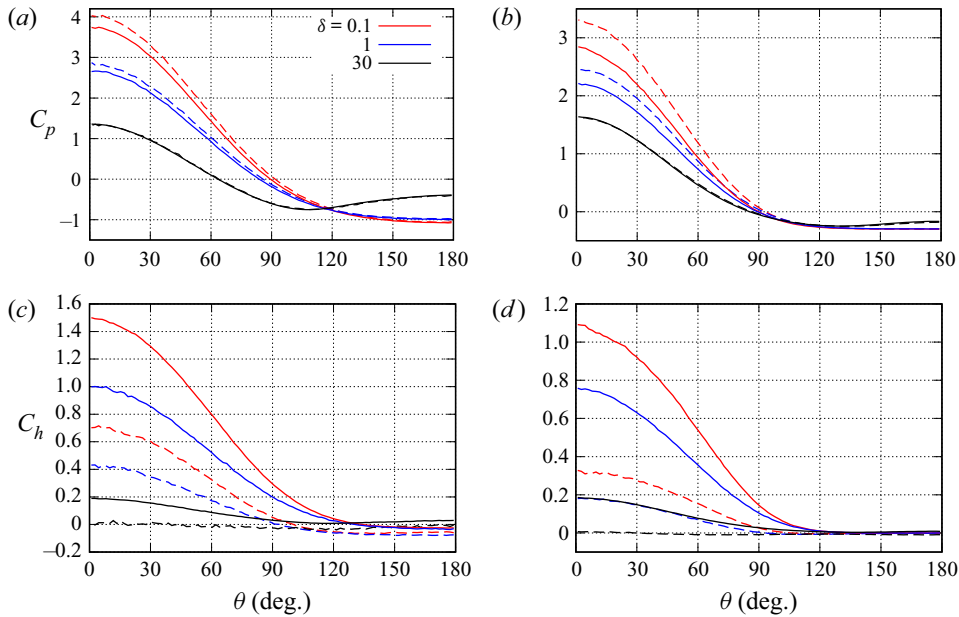
942 A17-24

Figure 9. (*a*,*b*) Pressure C_p and (*c*,*d*) energy transfer coefficients C_h versus angle θ for ^{4}He, diffuse scattering, $T_\infty = 300$ K: (*a*,*c*) $Ma = 1$; (*b*,*d*) $Ma = 2$. Solid lines indicate $T_w = 300$ K; dashed lines indicate $T_w = T_s$.

the small Mach number $Ma = 2$. The effect of T_w on C_h becomes more pronounced with decreasing Ma. The behaviours of the coefficients C_p and C_h at $Ma = 5$ and 10 similar to those at $Ma = 2$ are given in the supplementary material.

To demonstrate the sphere temperature effect on the flow field, the distributions of ^{4}He interacting diffusely with the cold sphere at $T_w = T_\infty = 300$ K are compared to those for the same gas at $T_w = T_s$ and $T_\infty = 300$ K in figure 10. In all situations, the sphere temperature affects strongly the temperature and density distributions near the sphere, while the gas velocity is affected weakly. In the case $Ma = 2$ and $\delta = 30$, the shock wave structure in front of the sphere is different for $T_w = T_s$ from that for $T_w = 300$ K. Mainly, the increase in the sphere temperature increases the distance between the sphere surface and bow shock.

The effect of the sphere temperature on flows of the other gases is very similar to that for helium because of the weak influence of the gas species, which was discussed in § 6.1.

7. Conclusions

The aerothermodynamic characteristics of a sphere in transonic, supersonic and hypersonic flows were calculated by the DSMC method employing AI potentials for interatomic collisions. The calculations have been performed for the noble gases ^{3}He, ^{4}He, Ne, Ar and Kr over a wide range of gas rarefaction spanning the free molecular, transitional and hydrodynamic flow regimes for Mach numbers 1, 2, 5 and 10. The parameters of the numerical scheme have been chosen to provide numerical errors in the drag and energy transfer coefficients less than 0.5 %. The effects of several factors, such as gas species, free stream temperature, sphere surface temperature and accommodation coefficients, were studied. The Cercignani–Lampis kernel for gas–surface interaction was used to describe
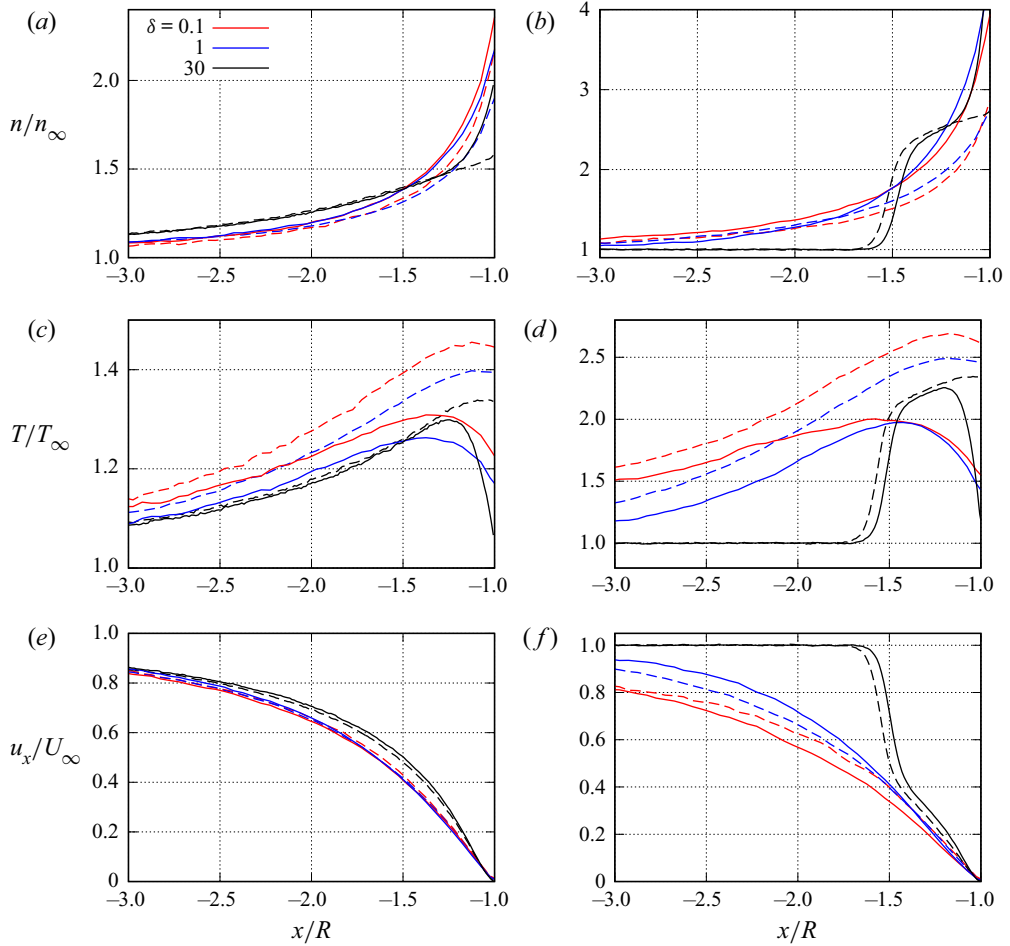
Figure 10. Axial distributions of (*a,b*) density n/n_∞, (*c,d*) temperature T/T_∞, and (*e,f*) velocity u_x/U_∞ for ^{4}He at $T_\infty = 300$ K and diffuse scattering: (*a,c,e*) $Ma = 1$; (*b,d,f*) $Ma = 2$. Solid lines indicate $T_w = 300$ K; dashed lines indicate $T_w = T_s$.

a non-diffuse reflection. The analysis of the numerical results leads to the following conclusions.

(i) The aerothermodynamic characteristics based on the AI potentials are significantly different from those based on the HS model at large values of the Mach number. The difference becomes smaller al low Mach numbers. For instance, the relative differences of the drag coefficient based on these two potentials are approximately 1.3 % and 10 % for Mach numbers 1 and 10, respectively. The relative difference of the energy transfer coefficient is almost three times larger. This conclusion is in agreement with the previous results for a gas flow past a cylinder by Volkov & Sharipov (2017).

(ii) The comparison of the results based on AI potentials points out a small divergence of the aerothermodynamic characteristics for different gases. The drag coefficient varies within 3 % at large Mach numbers, and within 1 % for Mach number 1.

The variation of the energy transfer coefficient is three-fold larger compared to that for the drag coefficient.

(iii) Both drag and energy transfer coefficients depend non-monotonically on the temperature of the free stream T_∞, assuming that the sphere temperature is equal to T_∞. The variation of the drag coefficient due to the variation of T_∞ is approximately 8 %, while the energy transfer coefficient varies within 15 %.

(iv) The diffuse gas–surface interaction always leads to the largest value of the energy transfer coefficient in comparison to the non-diffuse reflection model. The drag coefficient can be larger or smaller when the non-diffuse reflection is used instead of the diffuse one. Such behaviour is predicted by both the DSMC calculations in the transitional flow regime and theoretical equations obtained for free molecular flow. Both coefficients are strongly sensitive to the accommodation coefficients.

(v) When the surface temperature is increased, keeping the free stream temperature constant, the drag coefficient increases. The strongest effect of the sphere temperature is observed at the highest Mach number ($Ma = 10$), free molecular regime ($\delta = 0$), and diffuse gas–surface interaction. When the energy accommodation coefficient varies from 1 to 0.5, this effect becomes insignificant for all δ and Ma considered in the present work. Under the same conditions, the energy transfer coefficient decreases significantly and becomes negative in some situations.

Author ORCIDs.
 Felix Sharipov https://orcid.org/0000-0001-9372-2915.

REFERENCES

AMBRUS, V.E., SHARIPOV, F. & SOFONEA, V. 2020 Comparison of the Shakhov and ellipsoidal models for the Boltzmann equation and DSMC for *ab initio*-based particle interactions. *Comput. Fluids* **211**, 104637.

ASHLEY, H.J. 1949 Applications of the theory of free molecule flow to aeronautics. *J. Aeronaut. Sci.* **16**, 95–104.

AVLEEVA, V.K. 1970 Experimental study of heat transfer of a sphere and a flat plate in supersonic rarefied gas flow. *Fluid Dyn.* **5**, 339–343.

BAILEY, A.B. 1974 Sphere drag coefficient for subsonic speeds in continuum and free-molecule. *J. Fluid Mech.* **65**, 401–410.

BAILEY, A.B. & HIATT, J. 1971 Free-flight measurements of sphere drag at subsonic, transonic, supersonic, and hypersonic speeds for continuum, transition, and near-free-molecular flow conditions. *Tech. Rep.* AEDC-TR-70-291. Arnold Engineering Development Center.

BAILEY, A.B. & HIATT, J. 1972 Sphere drag coefficients for a broad range of Mach and Reynolds numbers. *AIAA J.* **10** (11), 1436–1440.

BATCHELOR, G.K. 2000 *An Introduction to Fluid Dynamics*. Cambridge University Press.

BERG, R.F. & BURTON, W.C. 2013 Noble gas viscosities at 25 °C. *Mol. Phys.* **111** (2), 195–199.

BIRD, G.A. 1994 *Molecular Gas Dynamics and the Direct Simulation of Gas Flows*. Oxford University Press.

BIRD, G.A. 2013 *The DSMC Method*.

CARLSON, D.J. & HOGLUND, R.F. 1964 Particle drag and heat transfer in rocket nozzles. *AIAA J.* **2**, 1980–1984.

CENCEK, W., PRZYBYTEK, M., KOMASA, J., MEHL, J.B., JEZIORSKI, B. & SZALEWICZ, K. 2012 Effects of adiabatic, relativistic, and quantum electrodynamics interactions on the pair potential and thermophysical properties of helium. *J. Chem. Phys.* **136** (22), 224303.

CERCIGNANI, C. 1972 Scattering kernels for gas–surface interactions. *Transp. Theory Stat. Phys.* **2** (1), 27–53.

CERCIGNANI, C. 1975 *Theory and Application of the Boltzmann Equation*. Scottish Academic Press.

CERCIGNANI, C. & LAMPIS, M. 1971 Kinetic model for gas–surface interaction. *Transp. Theory Stat. Phys.* **1**, 101–114.

CERCIGNANI, C., PAGANI, C.D. & BASSANINI, P. 1968 Flow of a rarefied gas past an axisymmetrical body. II. Case of a sphere. *Phys. Fluids* **11** (7), 1399–1403.

CHERNYAK, V.G. & SOGRABI, T.V. 2019 The role of molecule–surface interaction in thermophoresis of an aerosol particle. *J. Aerosol Sci.* **128**, 62–71.

CHERNYAK, V.G. & SOGRABI, T.V. 2020 The role of molecule–surface interaction in diffusiophoresis of a fine aerosol particle. *J. Aerosol Sci.* **144**, 105532.

CHING, E., BARNHARDT, M. & IHME, M. 2021 Sensitivity of hypersonic dusty flows to physical modeling of the particle phase. *J. Spacecr. Rockets* **58** (3), 653–667.

CROWE, C.T. 1967 Drag coefficient of particles in a rocket nozzle. *AIAA J.* **10**, 1021–1022.

CROWE, C.T., SOMMERFELD, M. & TSUJI, Y. 1998 *Multiphase Flows with Droplets and Particles*. CRC.

DIAS, F.C. & SHARIPOV, F. 2021 Shock waves structure propagating through heavy noble gases. Temperature dependence. *Shock Waves* **31** (6), 609–617.

DOGRA, V.K., MOSS, J.N., WILMOTH, R.G. & PRICE, J.M. 1994 Hypersonic rarefied flow past spheres including wake structure. *J. Spacecr. Rockets* **31** (5), 713–718.

DOGRA, V.K., WILMOTH, R.G. & MOSS, J.N. 1992 Aerothermodynamics of a 1.6-meter-diameter sphere in hypersonic rarefied flow. *AIAA J.* **30** (7), 1789–1794.

DRAKE, R.M. & BACKER, G.H. 1952 Heat transfer from spheres to rarefied gas in supersonic flow. *Trans. ASME* **74**, 1241–1249.

FERZIGER, J.H. & KAPER, H.G. 1972 *Mathematical Theory of Transport Processes in Gases*. North-Holland Publishing Company.

HELLMANN, R., BICH, E. & VOGEL, E. 2008 *Ab initio* potential energy curve for the neon atom pair and thermophysical properties of the dilute neon gas. I. Neon–neon interatomic potential and rovibrational spectra. *Mol. Phys.* **106** (1), 133–140.

HENDERSON, C.B. 1976 Drag coefficients of spheres in continuum and rarefied flows. *AIAA J.* **14** (6), 707–708.

HIRSCHFELDER, J.O., CURTISS, C.F. & BIRD, R.B. 1954 *The Molecular Theory of Gases and Liquids*. Wiley.

JÄGER, B., HELLMANN, R., BICH, E. & VOGEL, E. 2016 State-of-the-art *ab initio* potential energy curve for the krypton atom pair and thermophysical properties of dilute krypton gas. *J. Chem. Phys.* **144**, 114304.

KALEMPA, D. & SHARIPOV, F. 2020 Drag and thermophoresis on a sphere in a rarefied gas based on the Cercignani–Lampis scattering model of gas–surface interaction. *J. Fluid Mech.* **900**, A37.

KALEMPA, D. & SHARIPOV, F. 2021 Radiometric force on a sphere in a rarefied gas based on the Cercignani–Lampis model of gas–surface interaction. *Phys. Fluids* **33** (7), 073602.

KAVANAU, L.L. 1955 Heat transfer from spheres to a rarefied gas in subsonic flow. *Trans. ASME* **77**, 617–623.

KINGSLOW, M. & POTTER, J.L. 1963 Drag of spheres in rarefied hypervelocity flow. *AIAA J.* **1**, 2467–2473.

KOGAN, M.N. 1969 *Rarefied Gas Dynamics*. Plenum.

KOSHMAROV, Y.A. & SVIRSHEVSKII, S.B. 1972 Heat transfer from a sphere in the intermediate dynamics region of a rarefied gas (in Russian). *Izv. Akad. Nauk SSSR. Mekhan. Zhidk. Gaza*, No. 2, 170–172 (translation in *Fluid Dyn.* **7**, 343–346).

LANDAU, L.D. & LIFSHITZ, E.M. 1989 *Fluid Mechanics*. Pergamon.

LEA, K.C. & LOYALKA, S.K. 1982 Motion of a sphere in a rarefied gas. *Phys. Fluids* **25** (9), 1550–1557.

LOFTHOUSE, A.J., BOYD, I.D. & WRIGHT, M.J. 2007 Effects of continuum breakdown on hypersonic aerothermodynamics. *Phys. Fluids* **19** (2), 027105.

LORD, R.G. 1991 Some extensions to the Cercignani–Lampis gas–surface scattering kernel. *Phys. Fluids* A **3** (4), 706–710.

LOTH, E. 2008 Compressibility and rarefaction effects on drag of a spherical particle. *AIAA J.* **46** (9), 2219–2228.

LOTH, E., TYLER DASPIT, J., JEONG, M., NAGATA, T. & NONOMURA, T. 2021 Supersonic and hypersonic drag coefficients for a sphere. *AIAA J.* **59** (8), 3261–3274.

LOYALKA, S.K. 1992 Motion of a sphere in a gas: numerical solution of the linearized Boltzmann equation. *Phys. Fluids* **4** (5), 1049–1056.

MEIJA, J., *et al.* 2016 Isotopic composition of the elements 2013 (IUPAC technical report). *Pure Appl. Chem.* **88** (3), 293–306.

MELOSH, H.J. & GOLDIN, T.J. 2008 Heat and drag coefficients for reentry of impact ejecta. In *Lunar and Planetary Institute Science Conference Abstracts* (ed. S.J. Mackwell & E.K. Stansbery), vol. 39, p. 2457. Lunar and Planetary Institute.

NAGATA, T., NOGUCHI, A., NONOMURA, T., OHTANI, K. & ASAI, K. 2020 Experimental investigation of transonic and supersonic flow over a sphere for Reynolds numbers of 10^3–10^5 by free-flight tests with schlieren visualization. *Shock Waves* **30**, 139–151.

NAGATA, T., NONOMURA, T., TAKAHASHI, S. & FUKUDA, S. 2016 Investigation on subsonic to supersonic flow around a sphere at low Reynolds number of between 50 and 300 by direct numerical simulation. *Phys. Fluids* **28**, 056101.

NAGATA, T., NONOMURA, T., TAKAHASHI, S., MIZUNO, Y. & FUKUDA, S. 2018 Direct numerical simulation of flow around a heated/cooled isolated sphere up to a Reynolds number of 300 under subsonic to supersonic conditions. *Intl J. Heat Mass Transfer* **120**, 284–299.

NELSON, H.F. & FIELDS, J.C. 1996 Heat transfer in two-phase solid-rocket plumes. *J. Spacecr. Rockets* **33**, 494–500.

OZAWA, T., SUZUKI, T., TAKAYANAGI, H. & FUJITA, K. 2011 Investigation of Martian-dust drag and heat transfer for Mars sample return mission. *J. Thermophys. Heat Transfer* **25** (3), 341–353.

PAPADOPOULOS, P., TAUBER, M.E. & CHANG, I.-D. 1993 Heatshield erosion in a dusty Martian atmosphere. *J. Spacecr. Rockets* **30**, 140–151.

PARMAR, M., HASELBACHER, A. & BALACHANDAR, S. 2010 Improved drag correlation for spheres and application to shock-tube experiments. *AIAA J.* **48** (6), 1273–1276.

PATKOWSKI, K. & SZALEWICZ, K. 2010 Argon pair potential at basis set and excitation limits. *J. Chem. Phys.* **133**, 094304.

PETROV, V.A., RANJBAR, O.A., ZHILYAEV, P.A. & VOLKOV, A.N. 2020 Kinetic simulations of laser-induced plume expansion from a copper target into a vacuum or argon background gas based on *ab initio* calculation of Cu–Cu, Ar–Ar, and Ar–Cu interactions. *Phys. Fluids* **32**, 102010.

PORODNOV, B.T., KULEV, A.N. & TUKHVETOV, F.T. 1978 Thermal transpiration in a circular capillary with a small temperature difference. *J. Fluid Mech.* **88** (4), 609–622.

PORODNOV, B.T., SUETIN, P.E., BORISOV, S.F. & AKINSHIN, V.D. 1974 Experimental investigation of rarefied gas flow in different channels. *J. Fluid Mech.* **64** (3), 417–437.

PRZYBYTEK, M., CENCEK, W., KOMASA, J., ŁACH, G., JEZIORSKI, B. & SZALEWICZ, K. 2010 Relativistic and quantum electrodynamics effects in the helium pair potential. *Phys. Rev. Lett.* **104**, 183003 (erratum in Phys. Rev. Lett. **108**, 129902 (2012)).

RIAHIA, H., MELDIA, M., FAVIER, J., SERRE, E. & GONCALVES, E. 2018 A pressure-corrected immersed boundary method for the numerical simulation of compressible flows. *J. Comput. Phys.* **374**, 361–383.

SANSICA, A., ROBINET, J.-C., ALIZARD, F. & GONCALVES, E. 2018 Three-dimensional instability of a flow past a sphere: Mach evolution of the regular and Hopf bifurcations. *J. Fluid Mech.* **855**, 1088–1115.

SAUER, F.M. 1951 Convective heat transfer from spheres in a free molecule flow. *J. Aeronaut. Sci.* **18**, 353–354.

SCHAAF, S.A. & CHAMBRE, P.L. 1961 *Flow of Rarefied Gases*. Princeton University Press.

SEMYONOV, Y.G., BORISOV, S.F. & SUETIN, P.E. 1984 Investigation of heat transfer in rarefied gases over a wide range of Knudsen numbers. *Intl J. Heat Mass Transfer* **27** (10), 1789–1799.

SHARIPOV, F. 2003a Application of the Cercignani–Lampis scattering kernel to calculations of rarefied gas flows. II. Slip and jump coefficients. *Eur. J. Mech. B/Fluids* **22**, 133–143.

SHARIPOV, F. 2003b Application of the Cercignani–Lampis scattering kernel to calculations of rarefied gas flows. III. Poiseuille flow and thermal creep through a long tube. *Eur. J. Mech. B/Fluids* **22**, 145–154.

SHARIPOV, F. 2012 Benchmark problems in rarefied gas dynamics. *Vacuum* **86 SI** (11), 1697–1700.

SHARIPOV, F. 2016 *Rarefied Gas Dynamics. Fundamentals for Research and Practice*. Wiley-VCH.

SHARIPOV, F. 2017 *Ab initio* simulation of gaseous mixture flow through an orifice. *Vacuum* **143**, 106–118.

SHARIPOV, F. 2018a Influence of quantum intermolecular interaction on internal flows of rarefied gases. *Vacuum* **156**, 146–153.

SHARIPOV, F. 2018b Modelling of transport phenomena in gases based on quantum scattering. *Physica* A **508**, 797–805.

SHARIPOV, F. & BENITES, V.J. 2017 Transport coefficients of helium–neon mixtures at low density computed from *ab initio* potentials. *J. Chem. Phys.* **147**, 224302.

SHARIPOV, F. & BENITES, V.J. 2019 Transport coefficients of argon and its mixtures with helium and neon at low density based *ab initio* potentials. *Fluid Phase Equilib.* **498**, 23–32.

SHARIPOV, F. & BENITES, V.J. 2020 Transport coefficients of multi-component mixtures of noble gases based on *ab initio* potentials, viscosity and thermal conductivity. *Phys. Fluids* **32**, 077104.

SHARIPOV, F. & BENITES, V.J. 2021 Transport coefficients of isotopic mixtures of noble gases based on *ab initio* potentials. *Phys. Chem. Chem. Phys.* **23**, 16664–16674.

SHARIPOV, F. & BERTOLDO, G. 2006 Heat transfer through a rarefied gas confined between two coaxial cylinders with high radius ratio. *J. Vac. Sci. Technol.* A **24** (6), 2087–2093.

SHARIPOV, F. & DIAS, C.F. 2017 *Ab initio* simulation of planar shock waves. *Comput. Fluids* **150**, 115–122.

SHARIPOV, F. & DIAS, C.F. 2019 Temperature dependence of shock wave structure in helium and neon. *Phys. Fluids* **31**, 037109.

SHARIPOV, F. & MOLDOVER, M. 2016 Energy accommodation coefficient extracted from acoustic resonator experiments. *J. Vac. Sci. Technol.* A **34** (6), 061604.

SHARIPOV, F. & STRAPASSON, J.L. 2012*a* Direct simulation Monte Carlo method for an arbitrary intermolecular potential. *Phys. Fluids* **24** (1), 011703.

SHARIPOV, F. & STRAPASSON, J.L. 2012*b* *Ab initio* simulation of transport phenomena in rarefied gases. *Phys. Rev.* E **86** (3), 031130.

SHARIPOV, F. & STRAPASSON, J.L. 2013 Benchmark problems for mixtures of rarefied gases. I. Couette flow. *Phys. Fluids* **25**, 027101.

STORCH, J. 2002 Aerodynamic disturbances on spacecraft in free-molecular flow. *Tech. Rep.* TR-2003(3397)-1. Space and Missile Systems Center, U.S. Air Force Space Command (Los Angeles AFB, CA).

STRAPASSON, J.L. & SHARIPOV, F. 2014 *Ab initio* simulation of heat transfer through a mixture of rarefied gases. *Intl J. Heat Mass Transfer* **71**, 91–97.

TAGUCHI, S. 2015 Asymptotic theory of a uniform flow of a rarefied gas past a sphere at low Mach numbers. *J. Fluid Mech.* **774**, 363–394.

TAKATA, S., SONE, Y. & AOKI, K. 1993 Numerical analysis of a uniform flow of a rarefied gas past a sphere on the basis of the Boltzmann equation for hard-sphere molecules. *Phys. Fluids* A **5** (3), 716–737.

TROTT, W.M., CASTANEDA, J.N., TORCZYNSKI, J.R., GALLIS, M.A. & RADER, D.J. 2011 An experimental assembly for precise measurement of thermal accommodation coefficients. *Rev. Sci. Instrum.* **82** (3), 035120.

VASILEVSKII, E.B., OSIPTSOV, A.N., CHIRIKHIN, A.V. & YAKOVLEVA, L.V. 2001 Heat exchange on the front surface of a blunt body in a high-speed flow containing low-inertia particles (in Russian). *Izv. Akad. Nauk SSSR. Mekhan. Zhidk. Gaza*, vol. 76, no. 6, pp. 29–37 (translation in *J. Engng Phys. Thermophys.* **74** (6), 1399–1411).

VOGENITZ, F.W., BIRD, G.A., BROADWELL, J.E. & RUNGALDI, H. 1968 Theoretical and experimental study of rarefied supersonic flows about several simple shapes. *AIAA J.* **6** (12), 2388–2394.

VOLKOV, A.N. 2009 Aerodynamic coefficients of a spinning sphere in rarefied-gas flow (in Russian). *Izv. Akad. Nauk SSSR. Mekhan. Zhidk. Gaza*, vol. 44, no. 1, pp. 167–187 (translation in *Fluid Dyn.* **44**, 141–157).

VOLKOV, A.N. 2011 Transitional flow of a rarefied gas over a spinning sphere. *J. Fluid Mech.* **683**, 320–345.

VOLKOV, A.N. & SHARIPOV, F. 2017 Flow of a monatomic rarefied gas over a circular cylinder: calculations based on the *ab initio* potential method. *Intl J. Heat Mass Transfer* **114**, 47–61.

VOLKOV, A.N., TSIRKUNOV, Y.M. & OESTERLÉ, B. 2005 Numerical simulation of a supersonic gas–solid flow over a blunt body: the role of inter-particle collisions and two-way coupling effects. *Intl J. Multiphase Flow* **31**, 1244–1275.

WAGNER, W. 1992 A convergence proof for Bird's direct simulation Monte Carlo method for the Boltzmann equation. *J. Stat. Phys.* **66**, 1011–1044.

WALKER, A., MEHTA, P. & KOLLER, J. 2014 Drag coefficient model using the Cercignani–Lampis–Lord gas–surface interaction model. *J. Spacecr. Rockets* **51**, 1544–1563.

WALSH, M.J. 1977 Comment on 'Drag coefficient of spheres in continuum and rarefied flows'. *AIAA J.* **15** (6), 893–894.

WANG, M., AUDI, G., KONDEV, F.G., HUANG, W.J., NAIMI, S. & XU, X. 2017 The AME2016 atomic mass evaluation (II). Tables, graphs and references. *Chin. Phys.* C **41** (3), 030003.

WANG, X., ZHANG, Z., HAN, F., ZHANG, W. & ZHANG, S. 2022 *Ab initio* simulation of rarefied flows of gaseous mixtures in the system of microbeams with different temperatures. *Intl Commun. Heat Mass Transfer* **131**, 105872.

WEGENER, P.P. & ASHKENAS, H. 1961 Wind tunnel measurements of sphere drag at supersonic speeds and low Reynolds numbers. *J. Fluid Mech.* **10** (4), 550–560.

ZHU, L., WU, L., ZHANG, Y. & SHARIPOV, F. 2019 *Ab initio* calculation of rarefied flows of helium–neon mixture: classical vs quantum scatterings. *Intl J. Heat Mass Transfer* **145**, 118765.